Inertial Measurement Unit (IMU) Technology

Inverse Kinematics: Joint Considerations and the Maths for Deriving Anatomical Angles

Kai Daniel Oberländer, Dr. rer. nat.

September 2015

Table of Contents

Introduction

In recent years Inertial Measurement Units (IMU) have become a very important and wide spread sensor technology and its application areas span from industrial to ergonomical, biomechanical to life science and animation to virtual reality. Based on miniaturized and wireless transmission technology, one of main reasons for the high interest in IMU related technology is its ease of use, the light weight sensor technology and the mobile, camera independent use in field areas.

Contrary to its high potential in many application areas and easy and economical use, a very complex technical and mathematical background needs to be considered and applied users may benefit to study some technical aspects, general background principles and mathematical solutions prior to using the IMU technology. This is the main scope of this introduction booklet.

A future booklet will focus on the application techniques, methodological aspects, analysis possibilities and interpretation strategies in clinical, sports science and ergonomic investigations.

Mathematic Background

Quaternions

Quaternions are hyper-complex numbers of rank 4 and were first described by William Rowan Hamilton in 1843. A quaternion is a [4 × 1] matrix which consists of a scalar part **s** and a vector part **v**. They are widely used as attitude representation parameters of rigid bodies, such as those of a spacecraft. Based on Euler rotation theorem, the vector part is the normalized rotational axis **||e||** and the scalar part is based on the rotation/ transformation angle **θ**.

To determine the attitude of a rigid body's local coordinate system in three-dimensional space with respect to a reference system, a unit quaternion can be used.

The attitude of the local system is described by a quaternion. It describes the rotation of the local coordinate system aligned with the reference system to its final orientation by using a vector angle approach (Figure 1).

$$q = \begin{bmatrix} s \\ v_x \\ v_y \\ v_z \end{bmatrix} = \begin{bmatrix} q_s \\ q_x \\ q_y \\ q_z \end{bmatrix} = \begin{bmatrix} \cos\frac{\theta}{2} \\ \|\vec{e}\| * \sin\frac{\theta}{2} \end{bmatrix} \quad [1]$$

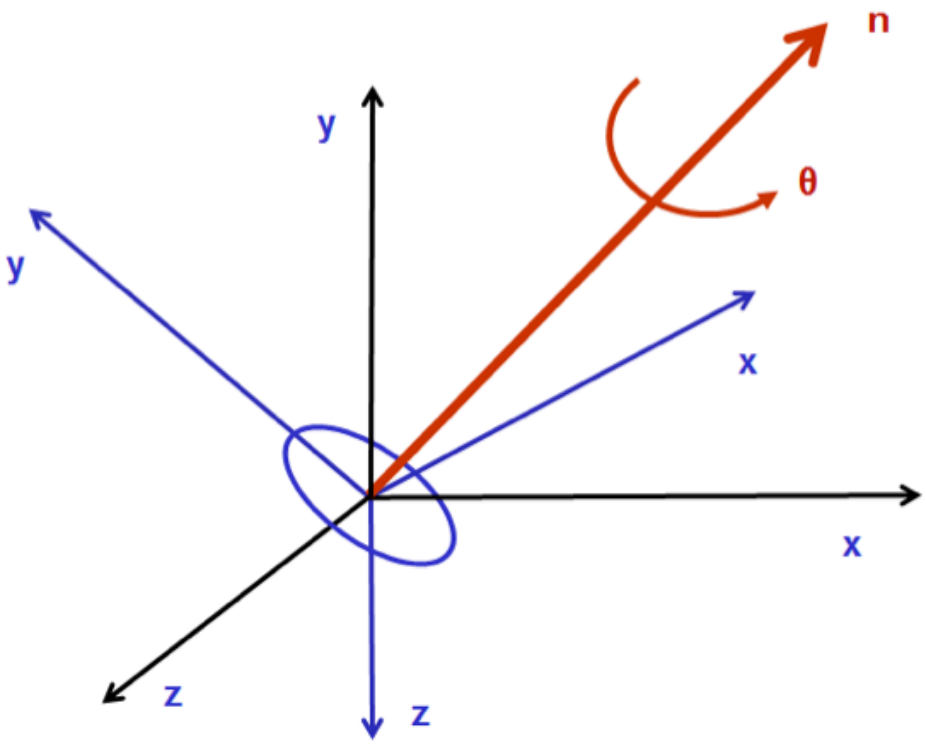

Figure 1: Quaternion attitude representation. The black coordinate system is the reference system and the blue coordinate system the local system. The quaternion (unit rotation vector **n** and rotation angle **θ**) describes the attitude offset between both systems.

Quaternion to rotation matrix

The conversion from quaternion q to a direction cosine matrix **R** is given in the equation:

$$R=\begin{bmatrix} q_s^2+q_x^2-q_y^2-q_z^2 & 2(q_x \cdot q_y-q_z \cdot q_s) & 2(q_x \cdot q_z+q_y \cdot q_s) \\ 2(q_x \cdot q_y+q_z \cdot q_s) & q_s^2-q_x^2 x q_y^2-q_z^2 & 2(q_y \cdot q_z-q_x \cdot q_s) \\ 2(q_x \cdot q_z-q_y \cdot q_s) & 2(q_y \cdot q_z+q_x \cdot q_s) & q_s^2-q_x^2-q_y^2+q_z^2 \end{bmatrix} \quad [2]$$

Advantages of the use of quaternions

A rotation in three dimensional space represented by a 3x3 matrix contains 9 elements (see section “Rotation Matrix and direction cosines”). A quaternion on the other hand is a 4-tuple. The use of quaternions therefore saves storage capacity, and its usage (e.g. multiplication, inverse rotation, addition) is computationally less intense.

Another advantage, especially in IMU settings, is the calculation of the attitude of the local coordinate system for the next time step by using the angular velocity data of the gyroscope directly. The calculation of a quaternion propagating with time is described by the following set of differential equations:

$$\dot{q}=\begin{bmatrix} \dot{q}_s \\ \dot{q}_x \\ \dot{q}_y \\ \dot{q}_z \end{bmatrix} = 0.5 \begin{bmatrix} q_s & -q_x & -q_y & -q_z \\ q_x & q_s & -q_z & q_y \\ q_y & q_z & q_s & -q_x \\ q_z & -q_y & q_x & q_s \end{bmatrix} \begin{bmatrix} 0 \\ w_x \\ w_y \\ w_z \end{bmatrix} \quad [3]$$

where **q’** is the attitude difference between the current quaternion **q** and new quaternion at the next time step, and $\boldsymbol{\omega_x}$, $\boldsymbol{\omega_y}$ and $\boldsymbol{\omega_z}$ are angular rates about the local **x**, **y** and **z** axes respectively.

Rotation matrix and direction cosines

Each unit vector **x** of the local system is represented by its components in the reference system (global or another local system). Dividing each component by the length of its vector (which is equal to 1) gives the cosine of the angle that the vector makes with each of the coordinate axes of the reference system. These angles are called the direction angles, and the cosines are termed the direction cosines. Direction cosines can be written in matrix form as elements of a [3 x 3] matrix. Therefore the notation $\mathbf{cos}_{(Y,z)}$ (see Eq. 4; same element as $\mathbf{Z}_{(2,3)}$ in Eq. 5) means the cosine of the angle formed by the second axis of the reference frame and the third axis of the local frame. Columns of the rotation matrix are [3 x 1] unit vectors, representing orientation of the local axis in the reference frame (global or another local system). The columns correspond to the axes of the local frame, and the rows of the matrix match the axes of the reference coordinate system.

$$R=\begin{bmatrix} \cos_{(X,x)} & \cos_{(X,y)} & \cos_{(X,z)} \\ \cos_{(Y,x)} & \cos_{(Y,y)} & \cos_{(Y,z)} \\ \cos_{(Z,x)} & \cos_{(Z,y)} & \cos_{(Z,z)} \end{bmatrix} \quad [4]$$

$$R=\begin{bmatrix} X_{(1,1)} & Y_{(1,2)} & Z_{(1,3)} \\ X_{(2,1)} & Y_{(2,2)} & Z_{(2,3)} \\ X_{(3,1)} & Y_{(3,2)} & Z_{(3,3)} \end{bmatrix} \quad [5]$$

Rotation matrix and projection angles

The projection angles are formed by (a) the projections of a local frame vector on the orthogonal planes of the reference frame and (b) the axes of the frame. Tangents of the projection angles can be easily represented through the direction cosines. For example, for the axis **x** of the local frame system:

$$\begin{aligned} \tan(YZ)_x &= \cos_{(Z,x)}/\cos_{(Y,x)} \\ \tan(YX)_x &= \cos_{(Y,x)}/\cos_{(X,x)} \\ \tan(XZ)_x &= \cos_{(X,x)}/\cos_{(Z,x)} \end{aligned} \quad [6]$$

where $\mathbf{tan(YZ)_x}$, $\mathbf{tan(YX)_x}$, and $\mathbf{tan(XZ)_x}$ are the tangents of the projection angles of the axis **x** of the local frame on the planes **YZ**, **YX**, and **XZ**, and $\mathbf{cos_{(Xx)}}$, $\mathbf{cos_{(Yx)}}$, and $\mathbf{cos_{(Zx)}}$ are the direction cosines of the angle formed by the axis x of the local frame and the axes X, Y, and Z of the reference frame. The projection angles are not independent. From Eq. 6, it follows that:

$$\tan(YZ)_x \cdot \tan(YX)_x \cdot \tan(XZ)_x = \frac{Z}{Y}\cdot\frac{Y}{X}\cdot\frac{X}{Z}=1 \quad [7]$$

Rotation matrix and Cardan angles

Finite rotations in three-dimensional space are non-commutative; in other words, they must be performed in a specific order. The change of orientation can be described as a sequence of three successive rotations from an initial position at which two reference frames coincide. Cardan angles are defined as three successive angles of rotation about a preset axis. In total, there are 12 sequences around floating and 12 around static axes of rotation.

By focusing on rotation sequences based on three different axes of rotation rather than using one axis twice the total set of sequences is reduced to a subset of 12 sequences.

The decomposition of a rotation Matrix **R** into a Cardan angle sequence **XY'Z"** is described by the following equations:

$$\begin{aligned} x &= \operatorname{atan2}(-R[2,3], R[3,3]) \\ y &= \operatorname{atan2}\left(R[1,3], \sqrt{R[3,3]^2+R[2,3]^2}\right) \\ z &= \operatorname{atan2}(-R[1,2], R[1,1]) \end{aligned} \quad [8]$$

Attitude Heading Reference System (AHRS)

An Inertial Measurement Unit (IMU) is based on gyroscopes and accelerometers, and makes it possible to track rotational and translational movements. However, measuring three-dimensional movements requires the sensors to register three mutually orthogonal axes. While IMUs can only measure an attitude relative to the direction of gravity, an AHRS, by combining an IMU and a three-axis magnetometer, is able to provide a complete measurement of orientation relative to both the direction of gravity and the earth's magnetic field.

Accelerometers

Accelerometers are devices used to sense a rigid body's acceleration due to the forces acting upon it. By integration of its measurements, velocity and distance can be computed; measuring these directly would require an external reference point. To measure acceleration in a three-dimensional setting, three accelerometers are mounted together orthogonally. In addition, it is also possible to construct a three-dimensional accelerometer using a single cubic mass and capacitive measurement in three directions. Accelerometers can be broadly subdivided into mechanical and solid state devices. Mechanical sensors are already well established and a large variety of them exists, whereas the potential of solid state devices is yet to be exploited. Furthermore, accelerometers can be divided into two groups: open-loop and closed-loop. The difference between the two groups is based on a simple operational characteristic: open-loop accelerometers have proof masses that are displaced, and that displacement is measured; closed-loop accelerometers' proof masses are maintained in a fixed position and the force (or current, power, etc.) necessary to maintain that position is measured.

Mechanical accelerometers

A simple mechanical accelerometer consists of a proof mass and a spring enclosed in a housing (Figure 2). It measures proper acceleration $\mathbf{a}_p = \mathbf{a} - \mathbf{g}$ (proper acceleration $\mathbf{a}_p$, acceleration **a**, gravity **g**) along one axis. The physical laws on which it is based are Hooke's law and Newton's second law of motion. Hooke's law states that the force required to extend or compress a spring is proportional to the distance **x** of the desired extension or compression. Consequently, the spring will create a force of the same magnitude to restore its original state, acting in the opposite direction of the applied force. The restoring force **F** can be described by **F = k*x**, where k is the spring's stiffness. Newton's second law of motion states that an object of mass m which is subjected to an acceleration exerts a force **F** such that **F = m*a**. It can therefore be concluded that,

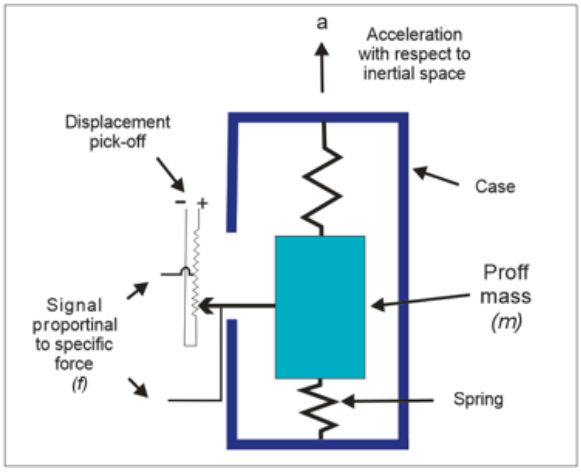

Figure 2: A simple accelerometer (adapted from Titterton & Weston, 2004)

since **F = m*a = k*x**, the accelerometer's mass m is displaced by **x = (m*a)*k**$^{-1}$. If the displacement, the spring's stiffness and the mass are known, it is possible to calculate the acceleration using **a = (k*x)*m**$^{-1}$.

A more precise measurement of acceleration is achieved by replacing the spring with electromagnetic coils. These coils are used to create a magnetic field, forcing the mass to remain in its original "null" position.

If a displacement of the mass occurs, a magnetic field is created by an electrical current running through the coils. This current is proportional to the acceleration (along the sensor's sensitive axis) acting upon the mass.

Force-feedback pendulous accelerometers

A wide range of mechanical accelerometers falls into the group known as force-feedback pendulous accelerometers. They generally consist of a pendulum with a proof mass attached to it or part of it. This pendulum is attached to the housing by a flexible component which is usually a pivot or hinge (Figure 3). Pick-off devices to detect pendulum motion are mostly optical, capacitive or inductive. The optical version uses a detector to measure the change of transmittance of a light beam running through the pendulum. The capacitive sensor type measures changes of capacitance between the pendulum and two electrodes by using a bridge circuit. The inductive system senses the differential current in two coils attached to the housing. The inductance of the coils is affected by a plate on the pendulum, and the relative position of the pendulum between the coils is measured instead of the "null"- position.

To restore the original position of the pendulum, two symmetrical coils are usually mounted onto it. Opposing these coils, two equal poles of two magnets are fixed to the housing. A current running through the coils will exert an electromagnetic force, maintaining the mass's original position and keeping the displacement at zero. This current will be proportional to the sensor's acceleration and, for most devices, this current will be the measurement, not the pick-off coils' signal. The case of this sensor type usually seals the other components hermetically, and is often filled with a low viscosity fluid to absorb shocks or vibrations.

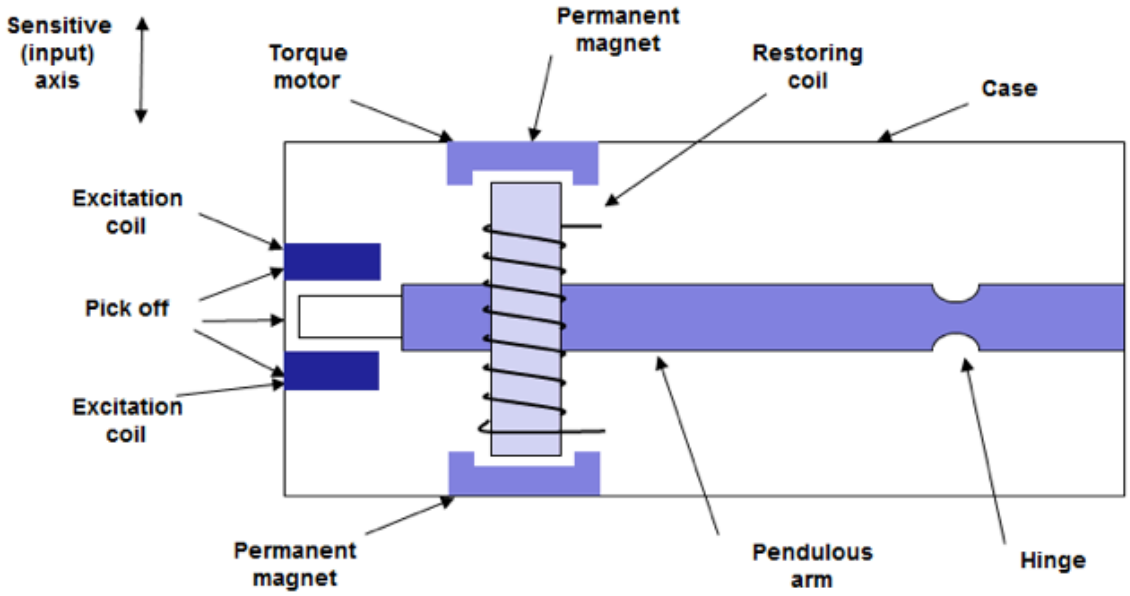

Figure 3: Force-feedback pendulum accelerometer (adapted from Titterton & Weston, 2004)

Solid State accelerometers

Solid states accelerometers use various phenomena to measure acceleration, with the goal of employing no moving mechanical parts in their construction.

Vibratory accelerometers

Vibratory accelerometers can be based on quartz-crystal technology. Two parallel quartz-crystal beams are attached to two separate proof masses (Figure 4). Each beam vibrates at its own resonant frequency along the input axis. At rest, the two frequencies are equal. However, when an acceleration along an axis parallel to the beams – i.e. the sensor's sensitive axis – occurs, one beam is compressed as the other one is stretched. This will change the beams' frequencies and the difference in frequency will be proportional to the acceleration along the sensitive axis.

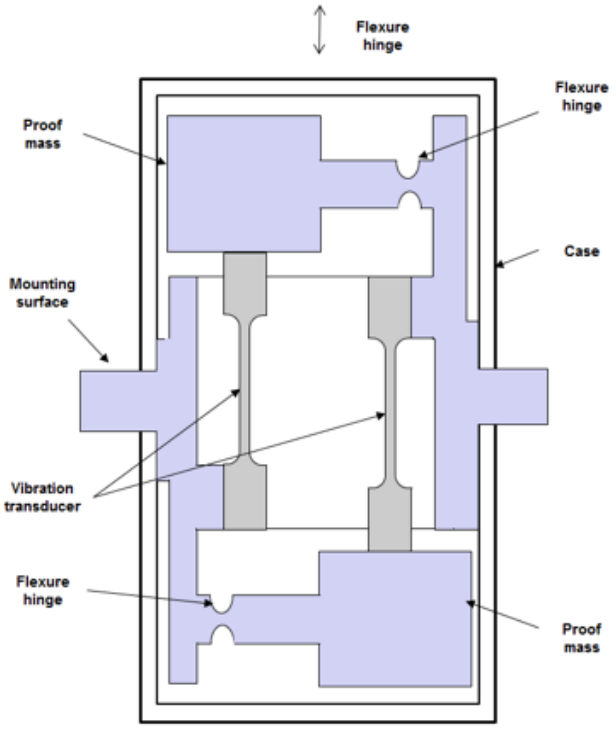

Figure 4: Vibrating beam accelerometer (adapted from Titterton & Weston, 2004)

Silicon accelerometers

In general, the accuracy of silicon accelerometers is not as high as that of other sensor types. However, they have the advantage of being very small, robust and inexpensive. They can be constructed using a cantilever beam made of silicon dioxide with a gold-coated end to form the proof mass. This cantilever is placed within a recess carved in a silicon substrate. The top of the cantilever is metal-plated to form one plate of a capacitor. The other plate is formed by the silicon substrate. As an acceleration along the sensor's sensitive axis occurs, there is a change in capacitance. In open-loop mode, the capacitance will be the measurand. Using this sensor in closed-loop mode provides greater sensitivity, with the current used to restore the cantilever's "null" position being proportional to the acceleration.

MicroElectroMechanical systems accelerometers (MEMS)

MEMS technology accelerometers are mostly based on the principle of pendulous accelerometers or the vibrating-beam types described above. The pendulous MEMS accelerometer consists of a hinged pendulous proof mass suspended by torsional spring flexures over a glass substrate. When the sensor is accelerated perpendicular to its plane, the proof mass performs a rotation, changing the capacitance between the proof mass and electrodes on an insulator substrate. The difference in capacitance is then proportional to the acceleration (206, 207). Resonant MEMS accelerometers resemble miniature versions of a similar working principle to that described for the vibrating beam sensors (Figure 5). These devices have been constructed using either silicon or quartz. A silicon version can be implemented by forming a monolithic vibrating tuning fork structure with a silicon proof mass on a glass substrate. Subjecting the sensor to an ac-

celeration in the direction of the vibration results in a change in resonant frequency. The oscillation and the sensing of the frequency are carried out by a silicon comb drive structure.

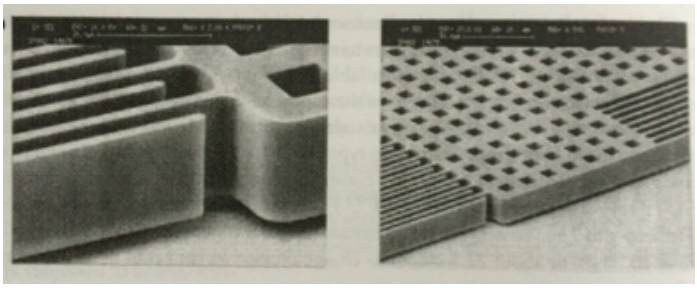

Figure 5: MicroElectroMechanical systems technology accelerometer (adapted from Titterton & Weston, 2004)

Gyroscopes

Gyroscopes in general are devices that measure either angular displacement (displacement gyroscopes) or angular rate of turn/angular velocity (rate gyroscopes). Most gyroscopes only measure along a single sensitive axis. Therefore, a combination of three orthogonally mounted gyroscopes is required to sense three-dimensional angular motion. For rate gyroscopes, the orientation of an object can be obtained by integration of the measured angular velocities.

Mechanical gyroscopes

Simple mechanical gyroscopes are based on gyroscopic inertia, Newton's second law of motion and conservation of angular momentum. Newton's second law of motion states that:

$$\tau = \frac{dL}{dt} = d\frac{(I \cdot \omega)}{dt} = I \cdot \alpha$$

where, τ is torque, L is the angular momentum vector, I is the moment of inertia, ω is the angular velocity vector and α is the angular acceleration vector. Conservation of angular momentum forces a rotating body to remain in its constant state if no torques are applied.

Simple mechanical displacement gyroscopes consist of a spinning wheel mounted in a set of gimbals that can rotate with respect to one another. The orientation of the wheel will remain constant in space and the orientation of the housing along all three axes with respect to the spinning wheel can be measured by angle measurement devices (Figure 6).

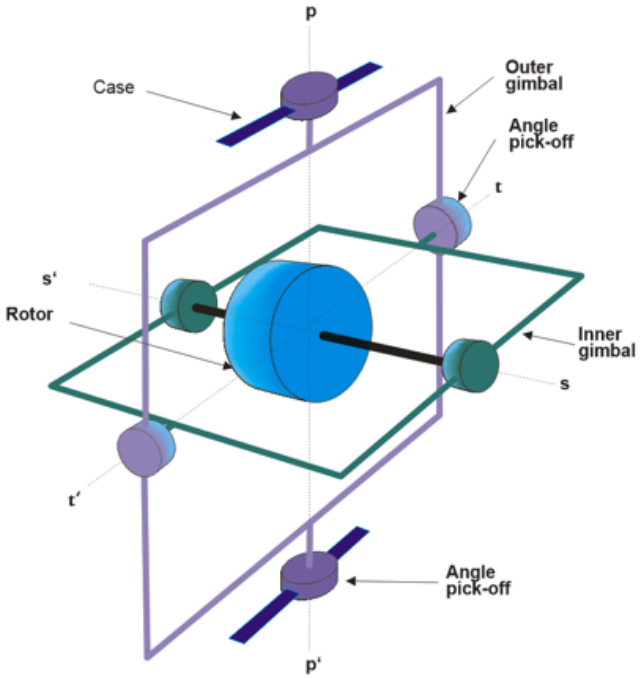

Figure 6: Schematic diagram of three-axis displacement gyroscope (adapted from Titterton & Weston, 2004)

Simple mechanical rate gyroscopes measure angular velocity along one axis. They can be implemented by a spinning wheel supported by a single gimbal inside a housing. In accordance with Newton's second law of motion, a torque will be applied to the wheel if a change in angular momentum occurs. This torque will force the wheel to process about the axis perpendicular to both the torque axis and the spin axis of the wheel. If the sensor is rotated about its input axis, a

torque about the output axis will be applied. A restraining spring will act against this torque and the angular change relative to a “null” position will be sensed by an angular pick-off device (Figure 7).

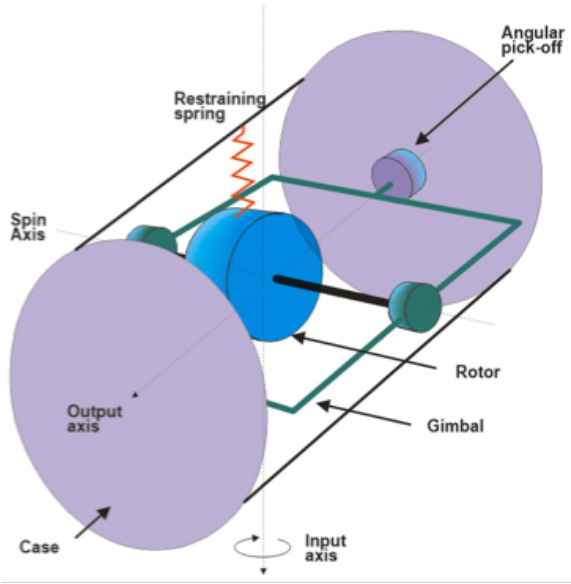

Figure 7: Schematic diagram of single-axis rate gyroscope (adapted from Titterton & Weston, 2004)

In practice, these sensors often operate in a closed-loop mode. The restraining spring is replaced by an electromagnetic torque generator to restore the “null” position. The current required to do so is proportional to the angular velocity.

Vibratory gyroscopes

Vibratory gyroscopes are based on a physical phenomenon called the Coriolis effect. This states that a force Fc acts upon an object of mass m when the object performs both a rotation and a translation. Fc is then perpendicular to the translation vector and can be described by Fc = -2*m (ω x v) (m = mass, ω = angular velocity, v = translational velocity).

The mass or masses of a vibratory gyroscope deliver a primary vibration and thus have an oscillatory linear velocity. If a rotation of the sensor about its sensitive axis (an axis which is perpendicular to the vibration) occurs, a secondary vibration is induced. This secondary vibration, which is created by the Coriolis force, is perpendicular to the first one and the displacement of the mass is proportional to ω. With known mass, primary vibration speed and displacement resulting from secondary vibration, it is possible to calculate angular velocity.

Tuning fork sensors

Tuning fork sensors are open-loop sensors and operate on the principle of basic vibratory gyroscopes. They consist of two masses attached to parallel quartz beams mounted on a single base (Figure 8). The masses are forced into a primary vibration 180° out of phase with one another. As a rotation about an axis parallel to the quartz beams occurs, the masses are pushed in and out of the primary vibration’s plane due to the Coriolis force.

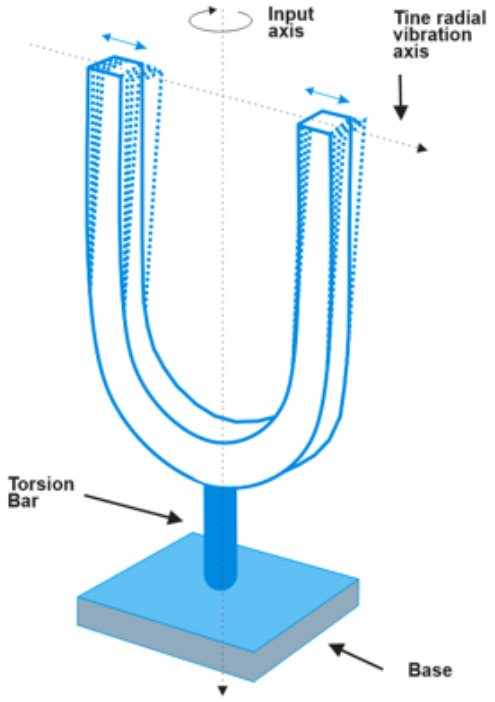

Figure 8: Principle of a tuning fork sensor (adapted from Titterton & Weston, 2004)

Quartz rate gyroscopes

Quartz rate sensors directly apply this method by combining two tuning forks as depicted in (Figure 9). Here, the primary vibration is generated in the driven tines. With a given angular velocity, the pick-up tines of the detector tuning fork develop a secondary vibration perpendicular to the plane of the primary one. This secondary vibration is then sensed by capacitor plates.

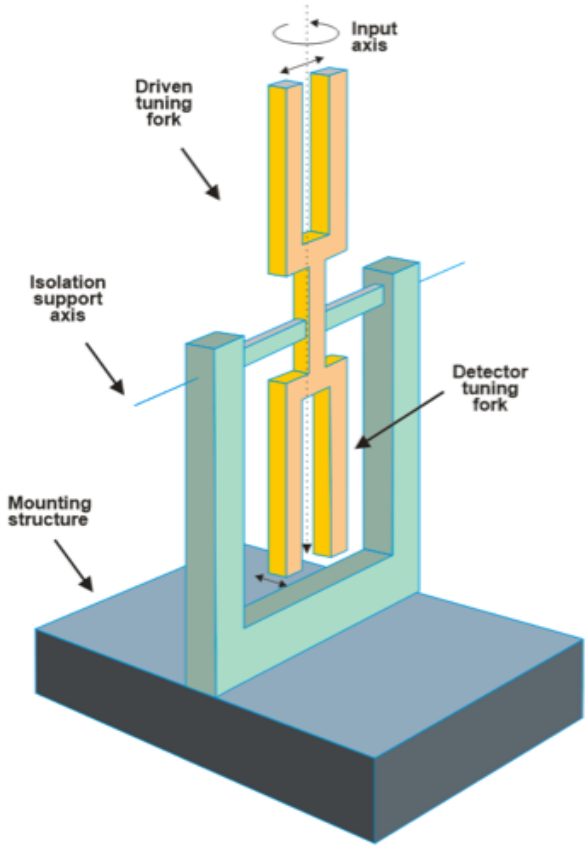

Figure 9: Principle of operation of a quartz rate sensor (adapted from Titterton & Weston, 2004)

Silicon gyroscopes

Gyroscopes made of silicon can be based on vibratory gyroscopes. The sensor discussed here is made up of two gimbals, one mounted within the other. The gimbals are mounted on pivots that allow them to perform a rotation about a certain axis. The axes through the gimbals' pivots are orthogonal to one another. The outer gimbal oscillates, driven by two electrodes. As the sensor rotates about its sensitive axis, an axis perpendicular to the sensor's plane, the inner gimbal will perform an oscillation of the same frequency. The magnitude of this oscillation will be proportional to the sensor's rate or rotation.

MicroElectroMechanical systems gyroscopes

Like ordinary vibratory gyroscopes, MEMS gyroscopes operate on the same principle of the Coriolis force acting upon a vibrating mass. Various implementations in MEMS technology for vibratory gyroscopes have been developed, such as silicon and quartz sensors. A tuning fork MEMS gyroscope can be realized by a silicon structure on a glass substrate. The silicon structure contains two masses which are forced to oscillate using motor drives. As an angular velocity occurs about the sensor's input axis, the masses are subject to a Coriolis force. The resulting secondary vibration is detected by capacitor plates. Quartz MEMS gyroscopes resemble a miniature version of the quartz rate sensors described above. The tuning forks consist of single-crystal piezoelectric quartz. The drive tines vibrate, driven by an oscillator. The pick-up tines then oscillate orthogonally to the primary vibration, creating an electrical signal which is proportional to the sensor's turning rate (Figure 10).

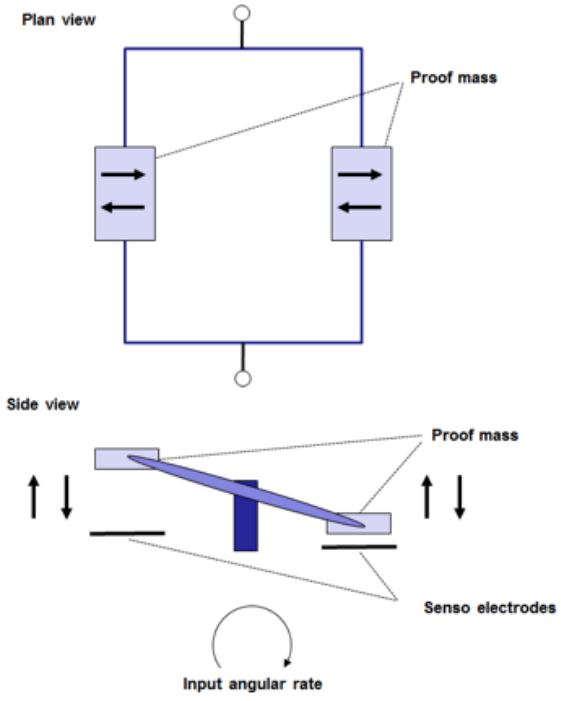

Figure 10: Motion of proof mass elements of a MEMS tuning fork gyroscope (adapted from Titterton & Weston, 2004)

Magnetometer

The basic idea of a magnetometer is to locate the magnetic north pole of the earth. The simplest example would be a magnetic compass, where a ferromagnetic element aligns with the earth's magnetic field. This happens because a magnetic moment will exert a torque upon a ferromagnet when it is placed inside a magnetic field. Since the surface of the earth is not parallel to its magnetic lines of force, there will be an angle between the needle of a horizontally aligned compass and the magnetic field lines. This angle is called dip angle and varies with the location on earth. The magnetic DIP angle can be measured by a compass free to rotate in the vertical plane (Figure 11).

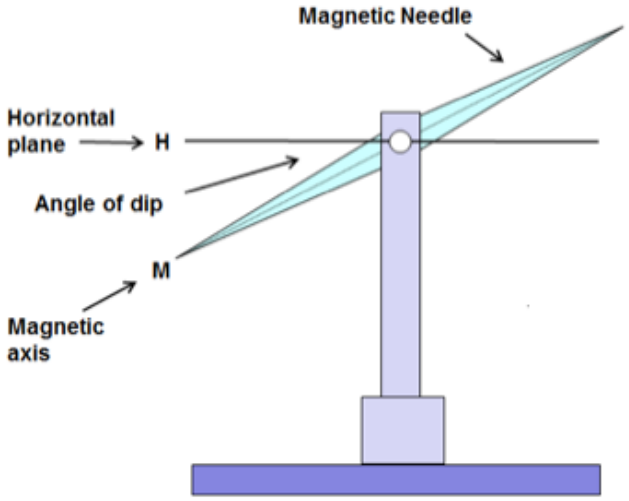

Figure 11: A compass free to rotate in the vertical plane measures the magnetic DIP angle

Electrical sensing devices take advantage of electromagnetic phenomena. Their output signal is usually proportional to the magnetic field along their sensitive axis. By combining three orthogonal sensors, it is possible to measure the magnitude of a magnetic field and to determine its direction, having measured its components along the three orthogonal axes of the sensors. A basic example of an electrical magnetometer is the fluxgate magnetometer. In the fluxgate magnetometer, a magnetically susceptible core lies within two excitation coils. An alternating current runs through one of the coils, magnetically saturating the core proportionally on alternate peaks of the signal. This magnetic field induces an electrical current in the second coil. In the absence of external magnetic fields, the induced signal will be proportional to the original current. However, if the sensor is subjected to an external magnetic field, the pick-up coil will experience altered current patterns. Measurement of the changes in the pattern is not easy to perform. Therefore, further development of the sensor brought up the following device: Two excitation coils are wound in opposition around two cores. A single pick-up coil is wrapped around both cores. The signal experienced by the pick-up coil will be zero due to the opposing magnetization of the cores. In the presence of a magnetic field, however, the output signal will be proportional to the magnitude of the magnetic field. For this set up, it is very important to match the cores and coils as precisely as possible, which is hard to accomplish in practice. For this reason, a device with a toroidal core wrapped in an excitation coil was introduced. A single coil used as a pick-up coil and a nulling coil perpendicular to the pick-up coil are wound over the toroid. This device can be operated in closed-loop mode, where a current in the nulling coil is used to compensate for the effect of the magnetic field.

Today, the most commonly used magnetometers are solid-state Hall effect sensors (Figure 12). The physical phenomenon they are based on is called the Hall effect, which describes the force exerted upon charge carriers of a current flowing through a conductor that is located in a magnetic field. Known as the Lorentz force, this force is orthogonal to both the direction of the current and the magnetic field. It forces the charge carriers to one side of the conductor, creating a voltage, called the Hall voltage:

$$V = A_h \frac{I \cdot B}{d}$$

where I is the current, B is the magnetic field, d is thickness of the sensor and Ah is a material constant called the Hall coefficient.

The detection of the Hall voltage has been shown to produce low outputs and to have low sensitivity and temperature stability. A more accurate approach therefore uses the displacement of a conductor caused by the Lorentz force.

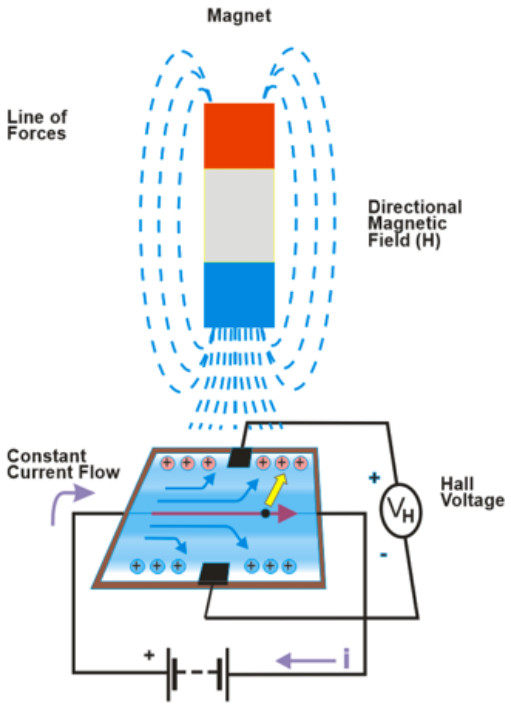

Figure 12: Hall effect sensor principles

One possible implementation of a magnetometer using MEMS technology is based on the Hall effect. It uses a low resistivity silicon structure suspended over a glass substrate by torsional beams. Above the silicon layer is an excitation coil with multiple turns. Below the silicon structure, two capacitor plates are fabricated directly upon the glass substrate (Figure 13). As a sinusoidal current is passed through the excitation coil in the presence of a magnetic field parallel to the sensor plane, the silicon structure will vibrate about the axis of the torsional beams. This is due to the opposing direction of the Lorentz force vectors, which are perpendicular to the vectors of both the magnetic field and the current, on either side of the excitation coil. The upward and downward movement of the silicon structure will cause a change in the capacitance of the two capacitors. One plate of each capacitor is formed by the silicon resonator, the other one by the plates on top of the glass substrate. The change in capacitance will be proportional to the magnetic field.

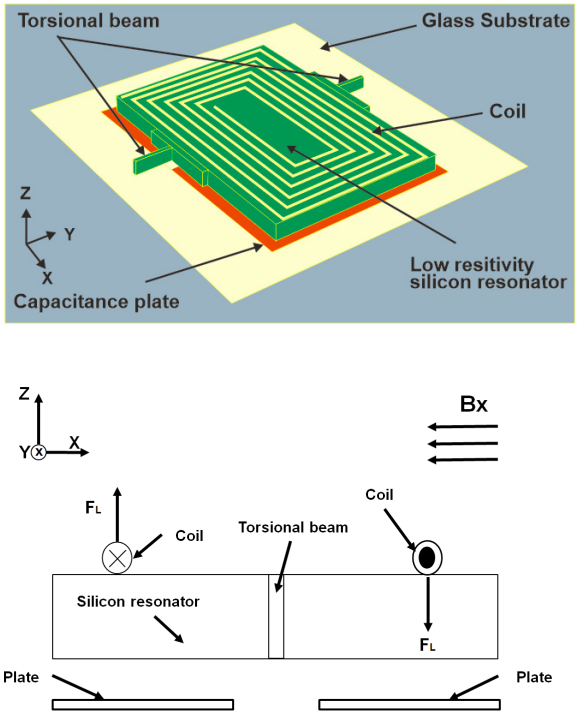

Figure 13: Structure and operating principle of the MEMS torsional resonant magnetometer.

Sensor fusion and Kalman filtering

An inertial measurement unit can be used to determine the attitude and change of attitude over time of an object in space. All of its sensors – namely three-dimensional accelerometers, three-dimensional gyroscopes and three-dimensional magnetometers – are required for this task. The use of gyroscopes allows the turn rates of the IMU about its local axis to be measured. In this way, a change in attitude of the unit can be detected. However, this measurement would be of little use if no initial position was known. Therefore, the initial attitude of the unit with respect to a reference system needs to be determined. The reference system regularly used is based on the direction of magnetic north and the direction of gravity, whereas the third axis is orthogonal to both of those and normally points east. To determine the initial orientation of the units with respect to this reference system, accelerometers and magnetometers are used.

Determining the sensor´s attitude in space

Prior to measurements of change of attitude, the sensors initial orientation has to be determined. This is done using measurements of the accelerometer and the magnetometer in a resting state (initial position).

To determine the initial roll and pitch angles of the IMU, the gravity vector within the accelerometer's local coordinate system is needed while the IMU is at rest. By using the distribution of gravity along the three orthogonal axes, the initial attitude of the IMU can be calculated. This approach is often described as "horizontal alignment" or "gravity alignment" and its maths/physics is demonstrated in Figure 14.

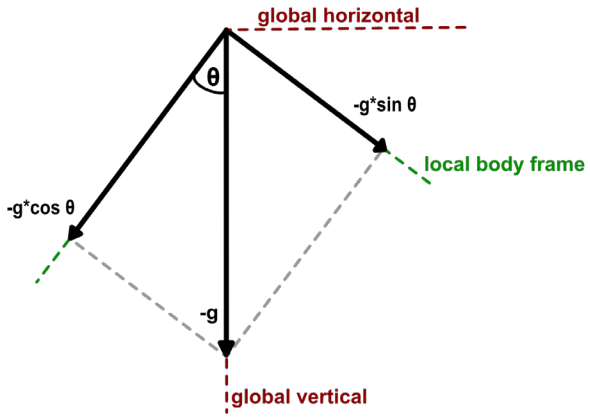

Figure 14: A schematic representation of a two dimensional gravity alignment. The x and y axes´ orientation in the global system are described by -gsinθ and -gcosθ respectively, where θ is the angle between the local system´s vertical axis and gravity.

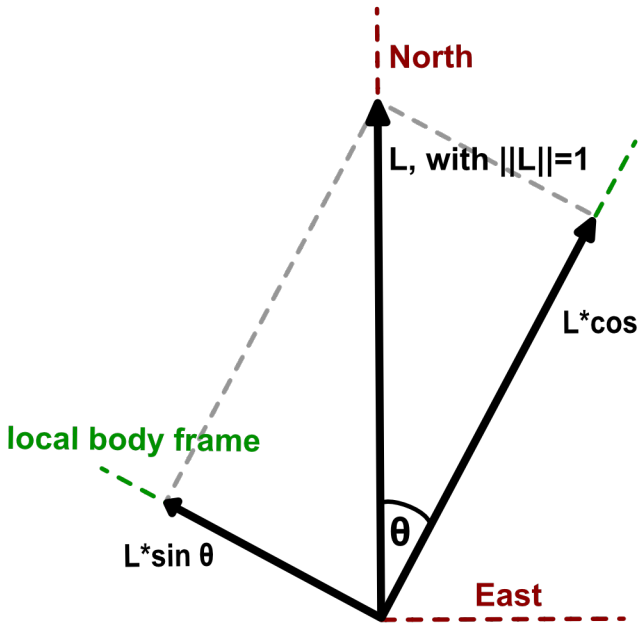

Figure 15: Determining orientation in the horizontal plane: x and y axis are described by L cos θ and L sin θ respectively.

In aircraft navigation, the heading is the angle between the direction that the nose of the aircraft is pointing and the vector of magnetic north in the horizontal plane. IMUs determine this angle by using their set of three orthogonal magnetometers to measure the distribution of the earth´s magnetic field among the three sensors. This measurement allows for a reconstruction of the vector of the magnetic field in the coordinate system of the IMU, and thus provides information of the sensor´s attitude in the horizontal plane or, in other words, its initial position with regard to the yaw axis. (Figure 15)

By combining the accelerometer and magnetometer approach while at rest, the initial attitude of the IMUs dimensional space with respect to the earth´s coordinate system can be determined.

Further changes in the sensor´s orientation are detected by the gyroscope. The angular velocity measured along its three axes is integrated (see section “Advantages of the use of quaternions”) once to determine the IMU´s orientation with respect to its initial position. By integrating the accelerometer signal once and twice, the change of velocity and position of the sensor, respectively, can be determined. The process of signal integration and hence attitude calculation and update is influenced by measurement errors, sensor calibration uncertainties and white noise, resulting in a biased attitude result and drift. Therefore, several optimization approaches have been developed to combine the information received from the gyroscope, accelerometer and magnetometer in order to overcome these problems (Madgwick, Harrison, & Vaidyanathan, 2011; Mazzà, Donati, McCamley, Picerno, & Cappozzo, 2012a; Zhou, Stone, Hu, & Harris, 2008).

Kalman filter

To increase the quality of IMU measurement data output and attitude calculation, a Kalman filter (Kalman, 1960) approach has often been used (Luinge & Veltink, 2005; Mazzà, Donati, McCamley, Pietro Picerno, & Cappozzo, 2012b; Sabatini, 2006). The basic Kalman filter is a mathematical algorithm for estimating a linear dynamic system´s state. It does this in two major steps. First it predicts the system´s next state based on the linear model taking into account the current state estimate. This prediction is then compared to the next measurement of state-related parameters, which are influenced by white noise and other uncertainties. A weighting of both prediction and measurement takes place and an estimate of the system´s optimized state as a combined variable of the two is created. The weighting is implemented by a so-called Kalman gain in the recursive part of the filter.

In relation to IMUs, this means that the output data, such as acceleration and orientation, are a combination of both the measurements recorded by the accelerometers and gyroscopes and a mathematical model which uses the previously determined state to predict the next one. The basic Kalman filter is limited to a linear assumption. More complex systems, however, can be nonlinear; for this reason, the extended Kalman filter has been developed and used in IMU settings (Sabatini, 2006). (Figure 16)

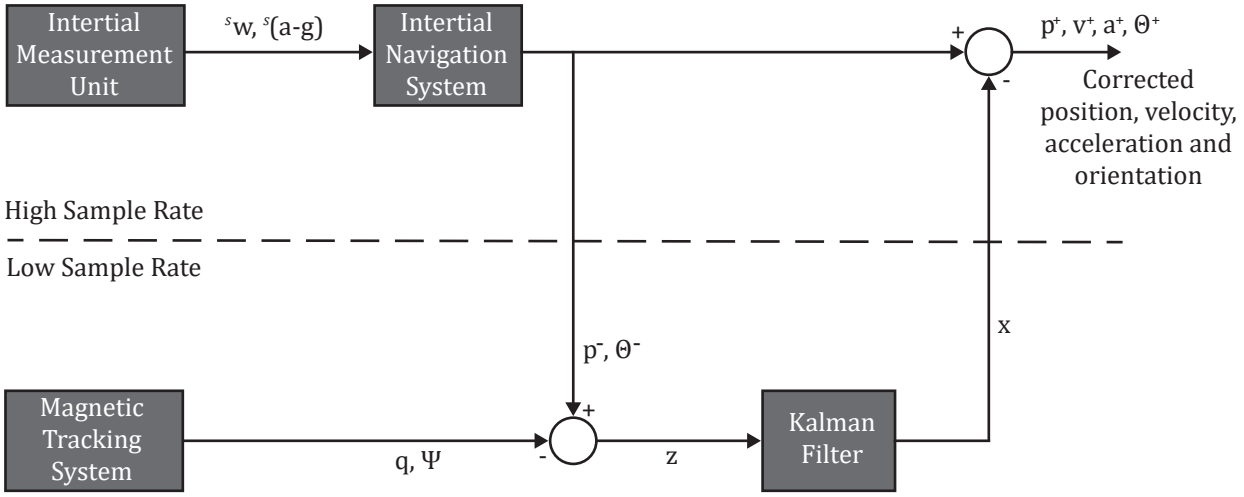

Figure 16: Kalman filter structure for combining inertial and magnetic measurements. Position p and attitude θ are estimated at a high sampling rate, using inertial navigation. At a lower rate, the magnetic system provides updates q and W. The differences between the two systems are delivered to the Kalman filter, which estimates the errors in the quantities of interest. These are used to correct position, velocity, acceleration, and orientation estimates, resulting in p, v, a, and θ, denoted by a 'plus' superscript. (Adapted from Roetenberg, Slycke, & Veltink, 2007).

Calculation of the Major Human Joint Angles

Sensor to body alignment

To express joint or segment kinematics in AHRS settings, the orientation of the sensors must be measured relative to a common reference frame (Grood & Suntay, 1983) and the relative orientation of the sensor to the attached body segment must be determined to correct angular offsets. To determine the sensor-to-segment alignment, several approaches has been developed (Favre, Jolles, Aissaoui, & Aminian, 2008; Favre et al., 2006; Roetenberg, 2006). One commonly used technique is to ask the subject to stand in an a priori known reference pose: a T-pose with straight legs, arms extended horizontally and thumbs forward, or a neutral-pose with arms beside the body. Assuming that each segment and joint is aligned to the reference pose, the offset rotation from the sensor in the global frame to the target orientation defined by the reference pose is determined by:

$$Q_S = Q_G * Q_C^{-1}$$

where, QS is the quaternion of the segment orientation in the global reference frame, QG is the quaternion of the sensor orientation in the global reference frame and QC is the offset quaternion of the sensor to the anatomical body frame.

The drawback of this approach is that the sensors could be affected by magnetic distortion, mostly affecting the horizontal reference direction (azimuth); the offset quaternion is therefore potentially not correct, resulting in a segment misalignment influencing the joint angle calculations. Another approach to determining the sensors-to-body orientation offset can be realized by using a reference movement and ignoring the information from the magnetometer. However, this approach is only suitable for single joint applications involving two segments. It has been previously reported in detail for calculating knee joint angles (Favre et al., 2008). The subject was asked to stand in a neutral upright body posture. Horizontal alignment of the IMU was achieved by aligning one axis of the embedded reference frame with the local vector of gravity. After alignment of the two IMUs to the global horizontal plane, the subject performed a predefined movement in one anatomical body plane (e.g. a hip abduction with straight legs). Assuming that both IMUs (shank and thigh) were subject to the same global angular velocity, a second axis of each IMU could be aligned to the average absolute local angular velocity vector. Hence, both IMUs were aligned to gravity and to the same global angular velocity during the movement, and were therefore represented in the same reference frame.

The cardan rotation sequence problem of inverse kinematics

It is well known that in 3D kinematic analysis, the computed segment orientations are dependent on the rotation sequence used in their reconstruction (Cappozzo, Croce, Leardini, & Chiari, 2005) In the reconstruction process to determine the orientation of a segment in space or in case of determine the relation of a segment to another segment, one axis has to be chosen first. Subsequently a second has to be chosen which then determines the identity of the third. A total of 6 floating and 6 statics sequences are possible when axes are selected in this way. The choice of cardan sequence strongly influences the values of segment orientation or joint angle calculations especially in the secondary planes of movement and is illustrated in Figure 17 while analyzing the same walking trail (1.6 m/s) of one subject with different cardan angle sets for the right knee joint.

To control this problem it is suggested to use one arbitrary convention (Wu and Cavanagh, 1995) or a rotation sequence that best reflects clinical requirements. For example, in many human actions the dominant movement axis is the flexion/extension, with less movement about abduction /adduction and internal/ external rotation axis. Therefore the flexion/extension axis should be considered as the first axis of rotation within a cardan rotation sequence (Cole, Nigg, Ronsky, & Yeadon, 1993; Grood & Suntay, 1983; Wu & Cavanagh, 1995). However each joint need to be addressed separately and general recommendations needs to be reviewed carefully if they are still be used within the scientific community and reflects the state of the art of clinical application.

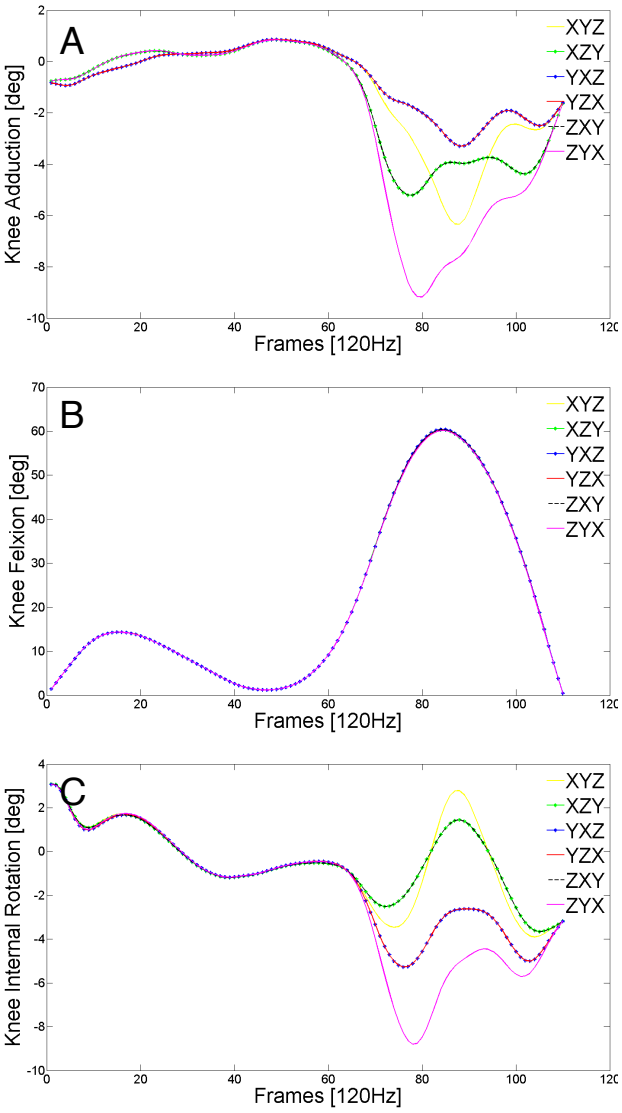

Figure 17: The Influence of different floating cardan rotation sequences for 3d knee angle calculation of the same walking trial (1.6 m/s) from one subject. Graph (A) shows the knee adduction/abduction angles; (B) the knee flexion angles and (C) knee internal/external rotation angles (data provided by the author; for additional information please see Woltring (1995) or visit http://isbweb.org/standards/dura.html).

The Hip

The hip joint (articulatio coxae) is a ball joint connecting the femur with the acetabulum (concave surface of the pelvis). It is able to support most of the body weight and, at the same time, gives the lower extremities a wide range of motion about several axes. The hip joint's range of motion allows the legs to be positioned in space; it is therefore vital for both effective human locomotion as well as for the precise movements required by different sports.

Healthy adults exhibit a range of motion about the sagittal axis of approx. 160°, with 140° flexion and 20° extension. Rotation about the anteroposterior axis varies depending on the hip joint's flexion angle, from 80° with a straight leg (50° abduction, 30° adduction, straight leg) to 100° with the hip flexed at 90° (80° abduction, 20° adduction). Internal and external rotation about the longitudinal axis allow a range of motion from 70° (30° external rotation, 40° internal rotation) with a straight leg to 90° (50° external rotation, 40° internal rotation) with the hip flexed at 90°.

The hip joint plays a crucial role in most daily activities as well as in sports, with high moments acting about it and influencing adjacent joints' kinetics (Pandy & Andriacchi, 2010). Impairment of any kind (e.g. muscular or bony) can have a great effect on gait kinematics and kinetics (Jacobsen et al. 2014) as well as quality of life, including comorbidities (Peter et al., 2015). Hip joint kinematics are also a excellent indicator of the body's reaction to a changed environment, such as altered ground characteristics (Horak & Nashner, 1986) or different kinds of shoes (Resende, Deluzio, Kirkwood, Hassan, & Fonseca, 2014).

Anatomical basics and definitions

This section is a brief refresher in skeletal anatomy and axis conventions of the hip joint and is related to Figure 18.

Definition of body segments and joints

P = pelvis

F = femur

HJ = hip joint, F relative to P

Hip joint angle calculation

Hip angle calculations are an essential part of lower extremity kinematics and have recently been used in many studies, e.g. for postural responses to surface perturbations (C.-L. Chen et al., 2014), analysis of taekwondo kicks (Y. K. Kim, Kim, & Im, 2011), investigation of joint force patterns in knee osteoarthritis patients (Nha et al., 2013), validation of imaging systems (Kapron et al., 2014), research on hip replacements (van Arkel, Modenese, Phillips, & Jeffers, 2013) and analysis of lower extremity reactions to perturbations (Oliveira et al., 2013).

Hip joint kinematics are generally calculated using the floating cardan sequence ZX'Y'', as proposed by the International Society of Biomechanics (Wu, 2002). The sequence assumes the following order of anatomical rotations:

1. Flexion/extension
2. Adduction/abduction
3. Internal/external rotation

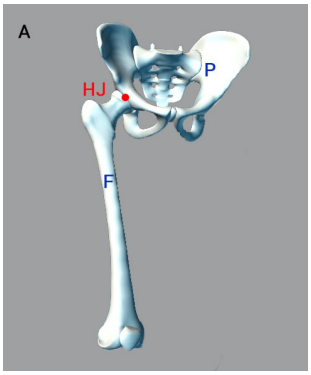

Figure 18: Anatomy of the hip joint with pelvis P, femur F and hip joint HJ.

The Knee

The knee joint (articulatio genus) is often considered as a hinge joint. However, this simplification does not represent the true kinematic nature of the largest and most complex joint in the human body. The knee connects the shank with the thigh and comprises two joints, namely the femorotibial joint (articulatio femorotibialis) connecting the femur and the tibia and the femoropatellar joint (articulatio femoropatellaris) which is the articulation between femur and patellar, the main function of which is to increase the moment arm of the knee extensors (Sherman, Plackis, & Nuelle, 2014).

The range of motion about the sagittal axis varies from 125° to 160° (120° to 150° flexion, 5° to 10° extension). About the longitudinal axis, the range of motion depends on the knee flexion angle and is at its highest at 90° flexion, reaching up to 70° (30° internal rotation, 40° external rotation). Rotation about the anteroposterior axis cannot be performed voluntarily; however, up to 15° angular changes occur during dynamic movements (Kernozek, Torry, & Iwasaki, 2008; McLean, Lucey, Rohrer, & Brandon, 2010). From a biomechanical perspective, the knee kinematics during locomotion are represented by a 6 DOF model, while rotation and translation (up to 20mm) take place about three independent axes (Papannagari et al., 2006; Tashman, Collon, Anderson, Kolowich, & Anderst, 2004).

Knee injuries such as ACL rupture, pain (including pain around the knee) and joint degeneration lead to altered knee mechanics, and instability influences motion patterns and the activity of a whole series of muscles during sports and daily life activities (Henriksen, Alkjaer, Simonsen, & Bliddal, 2009; Jenkyn, Hunt, Jones, Giffin, & Birmingham, 2008; Oberländer, Brüggemann, Höher, & Karamanidis, 2012; 2013; 2014). In addition, knee joint dynamics can reveal much valuable data, such as for analyzing amputees' recovery from falls (Curtze, Hof, Otten, & Postema, 2010) or dynamic stability during locomotion (Bosse et al., 2012). The analysis of knee movements is therefore a crucial part of lower extremity and whole body kinematics; it can aid our understanding of the influence of impairments, and can help determine important functional parameters.

Anatomical basics and definitions

This section is a brief refresher in skeletal anatomy and axis conventions of the knee joint and is related to Figure 19.

Definition of body segments and joints

F = femur

T = tibia

P = patella

Fi = fibula

K = knee joint, T relative to F

Knee angle calculation

Aging, muscle fatigue, and different pathologies like osteoarthritis (OA) or anterior cruciate ligament (ACL) rupture have been shown to alter knee kinetics and kinematics during gait. Using motion analysis to analyze such health restrictions or sport performance tasks, the choice of rotation sequence influences the values of joint orientation and may influence interpretation of data. To overcome this problem, some authors have suggested the consistent use of a single arbitrary convention (Wu & Cavanagh, 1995). Others prefer either a rotation sequence that best corresponds to clinical needs (Baker, 2001) or one that is most compatible with the actual type of motion being studied (Wu et al., 2005). Concerning the knee joint, the Grood and Suntay (Grood & Suntay, 1983) convention is well established in clinical settings (Oberländer et al., 2014; Papannagari et al., 2006) and for analyzing sport performance (C.-F. Lin, Hua, Huang, Lee, & Liao, 2015).

This convention is similar to the floating cardan sequence ZX'Y'' and means using the following order of the anatomical rotations:

1. Flexion/extension
2. Adduction/abduction
3. Internal/external rotation

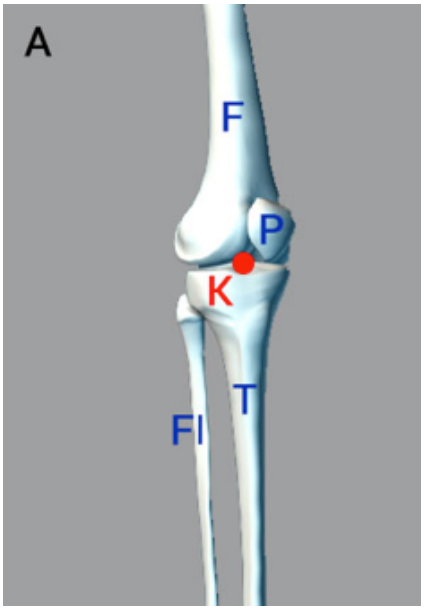

Figure 19: Anatomy of the knee joint with femur F, patella P, tibia T, fibula Fi and knee joint K.

The Ankle

The ankle-foot complex is the joint complex of most importance in locomotion. The joints of the ankle-foot complex most often studied are:

I. the talocrural joint (articulatio talocruralis), traditionally described as a hinge joint. However, based on the available literature, this varies from subject to subject, some showing a hinge pattern while others exhibit a varying kinematic pattern;

II. the subtalar joint (articulatio subtalaris), which is also often described as a hinge joint with a joint axis running from posterior, lateral, inferior, to anterior, medial, superior. This hinge axis may not be constant over the full range of motion under load; also, a different inclination angle of the joint axis has been reported between subjects, although this doesn't contradict the hinge-joint theory;

III. the transverse tarsal joint (Chopart's joint), comprising the talonavicular and calcaneocuboid joints. Both are often described as a closed kinematic chain with the subtalar joint;

IV. the metatarsophalangeal joint, the range of motion of which is important for the ankle dorsiflexion pattern beyond a certain level.

In describing the human ankle joint complex, which connects the shank (tibia and fibula) with the foot, Inman (Ahmad, Mam, & Sethi, 1989) pointed out that it can be functionally described as two separate joints: the talocrural joint and the subtalar joint. The complex permits three rotations that are usually labeled as plantar flexion and dorsiflexion, inversion-eversion and external-internal rotation, or abduction-adduction. The range of motion about the sagittal axis is approx. 80° (30° dorsiflexion, 50° plantar flexion). About the longitudinal axis of the foot, the range of motion is about 30° (10° eversion, 20° inversion), while values of 35° can be reached for both abduction and adduction of the foot (Grimston, Nigg, Hanley, & Engsberg, 1993). These secondary plane movements are mostly a product of rotations in both the talocrural and subtalar joints, because the movements of the two joints are coupled. Hence, humans aren't able to generate movement separately about these axes: motion in both joints usually occurs simultaneously during voluntary movements.

The role of the foot and hence the ankle joint complex is crucial to human locomotion. The ankle joint complex helps to properly position the foot in space, to keep balance (Hof, 2007) and to adapt to ground characteristics. For example, varying footwear and ground characteristics have been found to alter lower extremity kinetics (Willwacher, König, Potthast, & Brüggemann, 2013; Willwacher, Regniet, Mira Fischer, Oberländer, & Brüggemann, 2014) through altered ankle joint kinematics. Furthermore, the ankle, together with other structures of the distal part of the lower leg, is known to experience relatively high loads and is therefore thought to be more vulnerable than other parts of the leg during fast running (Petersen, Nielsen, Rasmussen, & Sørensen, 2014). In fact, many running related injuries are known to be located at the ankle (Lopes, Hespanhol Júnior, Yeung, & Costa, 2012). Therefore, altered and constrained ankle kinematics (e.g. congenital deformity of the foot), by preventing sufferers from walking normally, potentially causes dramatic restrictions in daily life (Cooper, Chhina, Howren, & Alvarez, 2014).

Because of the important role played by the foot and ankle in both support and propulsion, modern clinical and sport performance analysis often involves this segment and joint.

Anatomical basics and definitions

This section is a brief refresher in skeletal anatomy and axis conventions of the ankle joint and is directly related to Figure 20.

Definition of body segments and joints

T = tibia

F = fibula

Ta = talus

C = calcaneus

TJ = talocrural joint, T relative to Ta

SJ = subtalar joint, Ta relative to C

A = simplified ankle joint, foot relative to shank

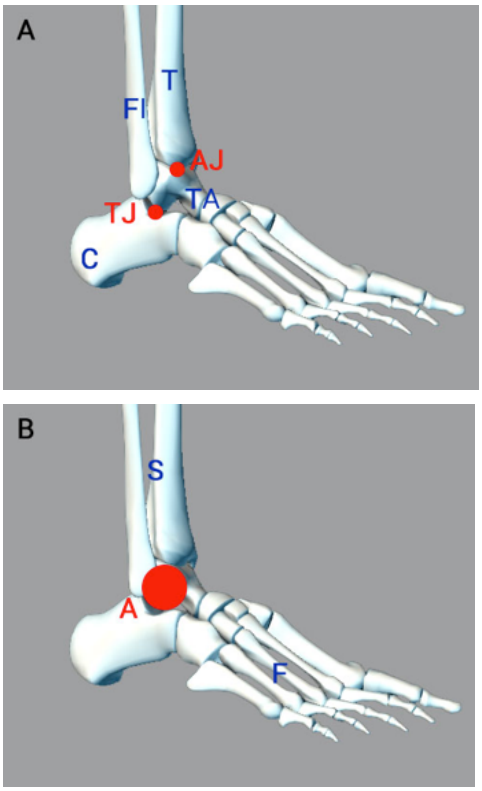

Figure 20: (A) Anatomy of the ankle with tibia T, fibula F, calcaneus C, talus Ta, talocrural joint TJ, subtalar joint SJ; (B) Simplified ankle joint complex with shank S, foot F and virtual ankle joint A

Ankle angle calculation

Because movement of the talus cannot be registered in living people by using external markers, the kinematics of the subtalar joint is hard to study. Accordingly, total mobility of the foot with regard to the shank is often proposed (van den Bogert, Smith, & Nigg, 1994; Wu, 2002), thereby addressing the needs of a great majority of the biomechanical community who are concerned with such functional activities as walking. In practice, this means the relative orientation of the calcaneus to the shank (Wu, 2002). This standard has recently been used in many studies, e.g. stroke rehabilitation (Deng et al., 2012), the effects of footwear on children's kinematics (Chard, Greene, Hunt, Vanwanseele, & Smith, 2013), diabetes gait analysis (Lewinson, Worobets, & Stefanyshyn, 2014; Rao, Saltzman, & Yack, 2006) and sports injury analysis (Bisseling, Hof, Bredeweg, Zwerver, & Mulder, 2007). According to the International Society of Biomechanics (Wu, 2002), the simplified ankle joint rotations should be calculated using the floating cardan sequence ZX'Y''. In anatomical terms, this means:

1. Flexion/extension,
2. Inversion/eversion, Adduction/abduction

However, for IMU applications, it seems more applicable to use the forefoot when describing global foot motion with respect to the shank, because the forefoot is more suitable for IMU attachment than the calcaneus.

The Trunk and Spine

Neck and back pain are among the most prevalent musculoskeletal conditions resulting in physical impairments and functional limitations (Chiu, Lam, & Hedley, 2005). It has been suggested that deficits in motor regulation and movement patterns might be contributing factors to the development of musculoskeletal dysfunction (Comerford & Mottram, 2001; Hodges & Moseley, 2003). Therefore, in recent years, intersegmental coordination between rhythmic leg, pelvis, trunk, arm and head movements has become an important focus of attention in the study of gait (Bianchi, Angelini, Orani, & Lacquaniti, 1998; Callaghan, Patla, & McGill, 1999; Cappozzo, 1983; Dietz, Zijlstra, & Duysens, 1994; Duysens & Van de Crommert HW, 1998).

The trunk makes up about 45% of body mass and its orientation (e.g. forward lean) is strongly responsible for positioning the center of mass in relation to the legs, thereby influencing the point of force application and direction and hence the lever arms of the ground reaction force vectors acting about the joints of the lower extremity (Oberländer et al., 2012).

The miniaturization of sensing, feedback, and computational devices has opened a new frontier for gait analysis and intervention (Shull, Jirattigalachote, Hunt, Cutkosky, & Delp, 2014). Wearable systems are portable and can enable individuals with a variety of movement disorders to benefit from analysis and intervention techniques that had previously been confined to research laboratories and medical clinics. Nevertheless, the application of sensors to the trunk is particularly challenging due to the difficulty in attaching any kind of technology to the vertebrae. It is therefore common to define kinematic chains in relation to the body anatomy, e.g. cervical spine, thoracic spine and lumbar spine. The ISB recommendation for an intersegmental vertebral angle convention is flexion/extension, lateral bending and axial rotation (Wu, 2002). This approach is often applied to relative orientation of the cervical spine, thoracic spine and lumbar spine to each other (Heyrman et al., 2013; Kiernan, Malone, Brien, & Simms, 2014; Pearcy & Hindle, 1989).

Summary:

Trunk or spinal angles should be calculated by using the following cardan rotation sequence:

1. Flexion/extension
2. Lateral bending
3. Axial rotation

The Shoulder

The shoulder can be seen as a perfect compromise between mobility and stability. The shoulder-joint complex allows for a large range of motion, well beyond that of the hip. Human upper-extremity range-of-motion covers almost 65% of a sphere (Engín & Chen, 1986) while the humerus can be axially rotated to almost any orientation within this space. The combination of both, to which can be added elbow flexion and pro/supination of the fore-arm, determine the working area of the hand.

The analysis of shoulder movement provides important information for the diagnosis and treatment of clinical disorders (Fayad et al., 2008), rehabilitation techniques (Hanratty et al., 2012), sports performance (Meyer et al., 2008) and injury prevention (Shaheen, Villa, Lee, Bull, & Alexander, 2013).

The calculation of 3D upper-limb motion analysis is normally carried out with the shoulder considered as a virtual thoracohumeral (TH) joint. The scapulothoracic (ST, virtual joint) and glenohumeral (GH) joints are not consid-ered individually despite the fact that scapular motion is a vital component of shoulder function. Indeed, during arm elevation in healthy subjects, there is significant motion of the scapula relative to the thorax with a mean 2° decrease in protraction, 39° increase in upward rotation and 21° increase in posterior tilt (Ludewig et al., 2009). Tracking of ST motion allows GH motion to be providing even more complete information on the function or dys-function of the entire shoulder girdle.

Anatomical basics and definitions

This section is a short refresher in skeletal anatomy and axis conventions of the shoulder joint complex and, for simplicity, is directly related to Figure 21.

Definition of body segments

C = clavicle

T = thorax

S = scapula

H = humerus

Joints of the shoulder complex

AC = acromioclavicular joint, S relative to C

SC = sternoclavicular joint, C relative to T

GH = glenohumeral joint, H relative to S

Important virtual joints

TH = thoracohumeral joint, H relative to T

ST = scapulothoracic joint, S relative to T

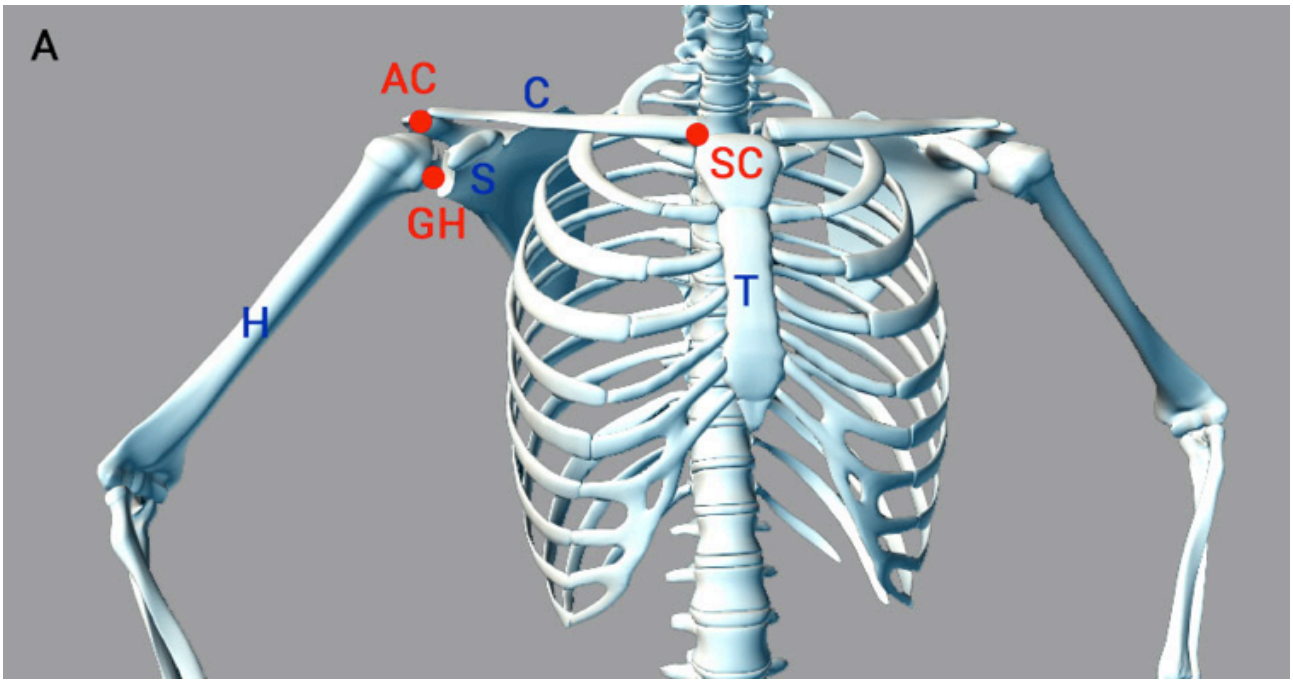

Figure 21: Anatomy and axis convention of the shoulder joint complex with humerus H, clavicle C, scapula S and acromioclavicular AC joint, glenohumeral GH joint and sternoclavicular SC joint

Shoulder angle calculation

From a methodological point of view, it is not possible (noninvasive applications) to calculate all joint angles of the shoulder complex (limited access to bony landmarks) therefore only ST, TH and GH are considered in this document.

General problems in calculation of scapulothoracic Kinematics

Simple marker-based techniques are subject to inaccuracies relating to the placement of markers or soft tissue artifacts (STAs) (Leardini, Chiari, Croce, & Cappozzo, 2005). This is particularly true when tracking scapular motion. The literature reports a difference of 87mm between the position of markers along the medial border of the scapula and the actual position of the scapula with the shoulder in full elevation (Matsui, Shimada, & Andrew, 2006).

Numerous studies have tried to optimize the calculation accuracy of scapulothoracic joint angle determination. A recent review (Lempereur, Brochard, Leboeuf, & Rémy-Néris, 2014) pointed out that an acromion marker cluster (AMC) method coupled with calibration of the scapula with the arm at rest is the most studied method.

Below 90°-100° of humeral elevation (abduction), this method is accurate to about 5° during arm flexion and 7° during arm abduction compared to palpation (good to excellent within-session reliability and moderate to excellent between-session reliability have been reported). Results obtained using the AMC method can be improved using multiple calibrations. Other methods using different marker locations or more markers on the scapula blade have been described but are less accurate than the AMC method (Lempereur et al., 2014).

Calculation of scapulothoracic joint

Single calibration method adapted for inertial measurement unit measurements

During the initial calibration (Karduna, McClure, Michener, & Sennett, 2001), the orientation of the scapula to the sensor is defined by a simple horizontal alignment or by user-specific inputs or offset measurements. The position of the sensor dramatically influences the results of scapula movements due to the different magnitude of soft tissue deformation errors (sliding of the sensor with respect to the underlying bone) at different locations on the scapula.

Multiple calibration method adapted for IMU measurements

A multi-calibrated approach (Brochard, Lempereur, & Rémy-Néris, 2011; Lempereur, Brochard, Mao, & Rémy-Néris, 2012) is used to increase the accuracy of measurements beyond 90° humeral elevation. The scapula orientation is measured (by an external device or palpation) during different static humeral abduction angles and recorded with respect to the scapula sensor. During dynamic tasks, a mapping function estimates the scapula orientation based on the static calibration data while measuring the sensor data on the scapula and correcting the orientation.

Scapulothoracic joint angles are generally calculated with respect to International Society of Biomechanics (Wu et al., 2005) recommendations by using the following rotation sequence YX'Z'':

1. External/internal rotation
2. Upward/downward rotation
3. Anterior/posterior tilting

Calculation of thoracohumeral joint kinematics

Due to the wide range of arm movements during different kinds of motor tasks, no principal plane of movement exists. Hence there is no general recommendation within the literature for joint angle calculation. In 2005, Wu et al. presented the International Society of Biomechanics (ISB) recommendation, a quasi-standard for calculating shoulder angles. They proposed an Euler angle sequence of YX'Y'' for thoracohumeral kinematics, which can create gimbal lock especially at 0° and 180° of humeral abduction (elevation). Moreover, rotation about the same axis twice does not seem meaningful in clinical settings and understanding. For this reason, the Euler angle sequence for thoracohumeral kinematics has been an oft-discussed controversy in recent years (Hill, Bull, Wallace, & Johnson, 2008; Lempereur et al., 2012; Šenk & Cheze, 2006). The latest scientific guidelines provide a task-based recommendation for calculating thoracohumeral joint angles (Lempereur et al., 2014).

Specifically, the use of the ZX'Y'' Euler sequence for the calculation of TH during flexion and the XZ'Y'' Euler sequence during abduction is recommended (Lempereur et al., 2014). In anatomically meaningful terms, this means that during movements where TH flexion is predominant the sequence should be:

1. Flexion/extension
2. Adduction/abduction
3. Internal/external rotation

During movements where TH abduction is predominant the sequence should be:

1. Adduction/Abduction
2. Flexion/extension
3. Internal/external rotation

Calculation of glenohumeral joint kinematics

Similar to the highlighted problems related to calculating joint angles of the thoracohumeral joint, glenohumeral joint kinematics are also often problematic to calculate. The ISB recommends the YX'Y'' sequence, resulting in the problems of gimbal lock and singularity described above. The alternate XZ'Y'' sequence has therefore been used frequently and successfully in recent publications (Levasseur, Tétreault, de Guise, Nuño, & Hagemeister, 2007; Ludewig & Cook, 2000; Phadke, Braman, LaPrade, & Ludewig, 2011). In anatomical meaningful terms that means:

1. Adduction/abduction
2. Flexion/extension
3. Internal/external rotation

Recommendations for biomechanical motion capture systems

Due to the dramatic effect of rotation sequence on angle calculations of the shoulder joint complex during different kinds of movement tasks, it seems to be valuable to provide different calculation methods in a post-processing manner to the user. The user should be able to select the appropriate rotation sequence based upon the recorded movement task.

For real-time calculations, it seems to be valuable to use projection angles or the helical axis convention (Hill et al., 2008) to provide a broadly acceptable joint angle calculation description, especially for GH joint angles during an average movement task.

For scapular tracking, a single calibrated AMC (Karduna et al., 2001) method is recommended, where the sensor is placed on the acromion and the body aligned to the neutral stance. The customer should be informed that this approach can only be used below 90° humeral elevation. In addition, sensor orientation (quaternions) should be provided to the user in order to enable user-specific approaches.

The Elbow

The elbow joint is one of the major joints of the upper extremities, comprising the humeroulnar joint (HU), humeroradial joint (HR) and proximal radioulnar joint (pRU) and connecting the upper arm with the forearm. Along with the shoulder and wrist it allows humans to position the hand in space by flexion/extension and pro-/supination (internal/external rotation of the forearm relative to the upper-arm) of the elbow. It thus makes it possible to effectively perform the motion tasks of daily life as well as high power movements e.g. in sports.

The range of motion of the elbow about its sagittal axis (flexion/extension) in healthy adults is approx. 140°-160° with 10° hyperextension and 130°-150° flexion. Rotation about the longitudinal axis (pro-/supination) can be carried out internal and external up to 90° resulting in a range of motion of 180°. The elbow is essentially a two-degree-of-freedom joint (flexion/extension and pronation/supination), with rotation about its antero-posterior axis (abduction/adduction) impossible to carry out voluntarily. Angular changes about that axis result from both a tilt in the flexion/extension axis and an angulation of the ulna and is therefore strongly related to the joint geometry (radius and curvature) of the elbow over the entire flexion/extension range of motion (Anglin & Wyss, 2000) and is often described as a passive angular change (Wu et al., 2005). The static carrying angle is a clinical measure of the abduction/adduction (varus/valgus angulation) of the arm with the elbow fully extended and the forearm full supinated (external rotation) and is between 5° to 15° in healthy men (Berme, Engin, & Silva, 1985) and 10° to 25° in healthy women (Schuind, An, Cooney, & Garcia-Elias, 1994).

Since the elbow joint plays an important role in upper limb movement, its impairment can have a dramatic effect on daily-life activities, resulting in compensatory moments (Kasten, Rettig, Loew, Wolf, & Raiss, 2009) and reduced quality of life.

Anatomical basics and definitions

This section is a brief refresher in skeletal anatomy and axis conventions of the elbow joint and is directly related to Figure 22.

Definition of body segments

H = Humerus

R = Radius

U = Ulna

Joints of the elbow

HU = humeroulnar joint, H relative to U

HR = humeroradial joint, H relative to R

RU = proximal radioulnar joint, R relative to U

Important virtual joint

FU = Forearm relative to humerus

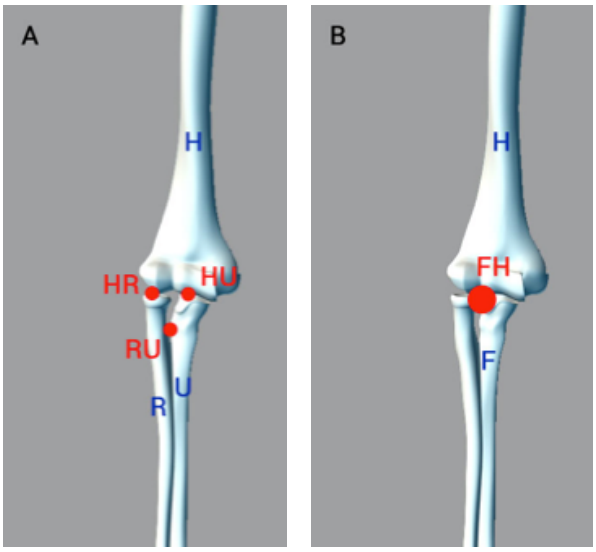

Figure 22: (A) Anatomy and axis convention of the elbow joint with humerus H, radius R, ulna U and humeroradial joint HR, humeroulnar joint HU, proximal radioulnar joint RU; (B) Simplified arm with humerus H, forearm F and virtual elbow joint FH.

Elbow angle calculation

Anatomically, flexion and extension of the elbow occurs in both the humeroulnar and humeroradial joints and pronation, and supination of the elbow are realized by the relative movement of the radius to the ulnar, involving rotations in both the proximal and distal radioulnar joints. From a methodological point of view, a simplification is needed due to the limited access to bony landmarks for attaching an Inertia Measurement Unit (IMU) and because of the relatively huge IMU footprint. The forearm, therefore, is often considered as a single rigid body with the elbow as a virtual ball joint enabling the motion of the forearm relative to the humerus. This simplification is in line with the International Society of Biomechanics recommendation and often used in recent studies involving upper extremity biomechanics such as analyzing activities of daily living (Aizawa et al., 2010), movements of patients with upper extremity disorders (Kasten et al., 2009), sports movements (Robert, Rouard, & Seifert, 2013), orientation sense (King, Harding, & Karduna, 2013), aging effects (Xu, Qin, Catena, Faber, & Lin, 2013) and IMU mathematics optimization approaches (Lambrecht & Kirsch, 2014).

As proposed by the International Society of Biomechanics (Wu et al., 2005), elbow joint angles are generally calculated using the a floating cardan sequence ZX'Y'', which correspond to anatomical rotations in the following order:

1. Flexion/extension
2. Adduction/abduction
3. Pronation/supination

The Wrist

The wrist is a complex of two joints connecting the forearm with the hand. The more proximal of the two (articulatio radiocarpalis) connects the first row of carpal bones (scaphoid carpal, lunate carpal and triquetral carpal) with the radius. The farther distal one (articulatio mediocarpalis) is an S-shaped joint and lies between the first and second row (trapezium carpal, trapezoid carpal, capitate carpal and hamate carpal) of carpal bones. These two joints connect the forearm with the hand and make it possible to voluntarily rotate the hand about two axes (flexion/extension and abduction/adduction). The range of motion about the flexion/extension axis varies from 100°-140° and is realized in both joints, whereas rotations about the abduction/adduction axis are carried out in the articulatio radiocarpalis and ranges from 50°-60°. Pronation and supination are not carried out in in the wrist joint but take place in the distal radioulnar joint (articulatio radioulnar distalis) as a movement of the radius relative to the ulna. The ulna itself is not directly involved in the wrist but only connected to it by an articular disc.

Wrist movements play an important role in sports and everyday activities, allowing the hand to be precisely positioned in order to carry out specialized tasks like writing, grasping and even gesturing.

Anatomical basics and definitions

This section is a brief refresher in skeletal anatomy and axis conventions of the wrist and is directly related to Figure 23. For simplification purposes, the carpal bones have been summarized into the first row of carpal bones C1 (articulatio radiocarpalis) and the second row C2 (articulatio mediocarpalis).

Definition of body segments

R = Radius

U = Ulna

C1 = Scaphoid carpal, lunate carpal and triquetral carpal (left to right)

C2 = Trapezium carpal, trapezoid carpal, capitate carpal and hamate carpal (left to right)

M = 3rd metacarpal

Joints of the wrist

Radiocarpal joint (articulatio radiocarpalis)

Mediocarpal joint (articulatio mediocarpalis)

Virtual wrist joint

HF = hand relative to forearm

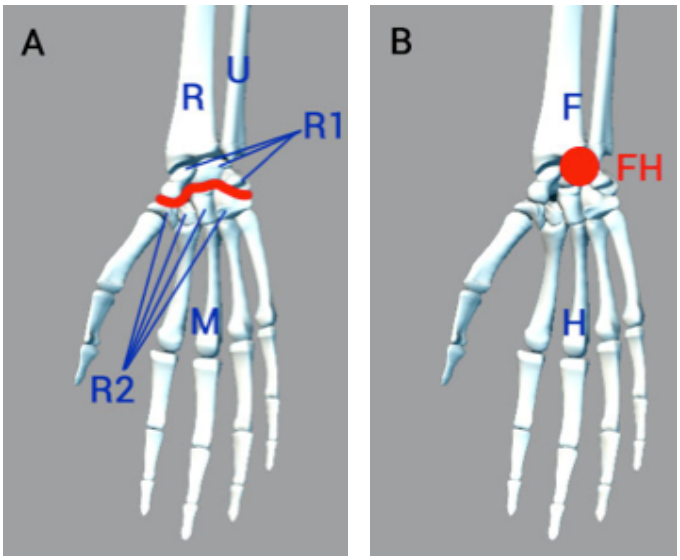

Figure 23: (A) Anatomy and axis convention of the wrist with radius R, ulna U, first row of carpal bones R1, second row of carpal bones R2 and 3rd metacarpal M; articulatio mediocarpalis highlighted as the red line; (B) Simplified arm with forearm F, hand H and virtual wrist joint HF

Wrist joint angle calculation

Because it can be difficult to analyze movements of each bone of the hand due to the very small anatomical landmark clearances, a simplified model of the wrist joint is needed, in particular in IMU motion capture applications. (Wu et al., 2005), as part of the ISB recommendations, proposed a model treating the hand as a single rigid body whose motion is described using a virtual joint relative to the forearm In this model, the center of the third metacarpal bone serves as the origin of the embedded hand coordinate system. Despite the fact that the distal radioulnar joint is anatomically not part of the wrist joint, it is considered in this simplified model to describe pronation and supination of the hand relative to the forearm. The simplified model also allows the use of Inertial Measurement Units (IMUs), overcoming the size issues usually encountered, and is frequently employed for analyzing upper extremity biomechanics such as general research on wrist dynamics (Peaden & Charles, 2014) in clinical studies of wheelchair propulsion (Schnorenberg et al., 2014) and for analyzing sports movements (Robert et al., 2013).

According to the International Society of Biomechanics proposal (Wu et al., 2005), wrist joint angles should generally be calculated in the following ZY'X'' order:

1. Flexion/extension
2. Adduction/abduction
3. Pronation/supination

Table of Figures

References

Ahmad, S., Mam, M. K., & Sethi, T. S. (1989). Patellar tendon bearing plaster casts in fractures of the tibia. *International Orthopaedics, 13(*4), 247–251. http://doi.org/10.1007/BF00268506

Aizawa, J., Masuda, T., Koyama, T., Nakamaru, K., Isozaki, K., Okawa, A., & Morita, S. (2010). Three-dimensional motion of the upper extremity joints during various activities of daily living. *Journal of Biomechanics, 43*(15), 2915–2922. http://doi.org/10.1016/j.jbiomech.2010.07.006

Anglin, C., & Wyss, U. P. (2000). Review of arm motion analyses. Proceedings of the Institution of Mechanical Engineers Part H, *Journal of Engineering in Medicine, 214*(5), 541–555. http://doi.org/10.1243/0954411001535570

Baker, R. (2001). Pelvic angles: a mathematically rigorous definition which is consistent with a conventional clinical understanding of the terms., *13*(1), 1–6.

Berme, N., Engin, A. E., & Silva, K. M. C. D. (1985). Biomechanics of normal and pathological human articulating joints. Dordrecht ; Boston : Nijhoff ; Hingham, MA, USA : Distributors for the United States and Canada, Kluwer Boston.

Bianchi, L., Angelini, D., Orani, G. P., & Lacquaniti, F. (1998). Kinematic coordination in human gait: relation to mechanical energy cost. *Journal of Neurophysiology, 79*(4), 2155–2170.

Bisseling, R. W., Hof, A. L., Bredeweg, S. W., Zwerver, J., & Mulder, T. (2007). Relationship between landing strategy and patellar tendinopathy in volleyball. *British Journal of Sports Medicine, 41*(7), e8. http://doi.org/10.1136/bjsm.2006.032565

Bosse, I., Oberländer, K. D., Savelberg, H. H., Meijer, K., Brüggemann, G.-P., & Karamanidis, K. (2012). Dynamic stability control in younger and older adults during stair descent. *Human Movement Science, 1–11.* http://doi.org/10.1016/j.humov.2012.05.003

Brochard, S., Lempereur, M., & Rémy-Néris, O. (2011). Double calibration An accurate, reliable and easy-to-use method for 3D scapular motion analysis. *Journal of Biomechanics, 44*(4), 751–754. http://doi.org/10.1016/j.jbiomech.2010.11.017

Callaghan, J. P., Patla, A. E., & McGill, S. M. (1999). Low back three-dimensional joint forces, kinematics, and kinetics during walking. Jclb, *14*(3), 203–216.

Cappozzo, A. (1983). The forces and couples in the human trunk during level walking. *Journal of Biomechanics, 16*(4), 265–277.

Cappozzo, A., Croce, Della, U., Leardini, A., & Chiari, L. (2005). Human movement analysis using stereophotogrammetry. Part 1: theoretical background, *21*(2), 186–196. http://doi.org/10.1016/j.gaitpost.2004.01.010

Chard, A., Greene, A., Hunt, A., Vanwanseele, B., & Smith, R. (2013). Effect of thong style flip-flops on children's barefoot walking and jogging kinematics. Journal of Foot and Ankle Research, 6(1), 8. http://doi.org/10.1186/1757-1146-6-8

Chen, C.-L., Lou, S.-Z., Wu, H.-W., Wu, S.-K., Yeung, K.-T., & Su, F.-C. (2014). Effects of the type and direction of support surface perturbation on postural responses. *Journal of NeuroEngineering and Rehabilitation, 11*(1), 50. http://doi.org/10.1186/1743-0003-11-50

Chiu, T. T., Lam, T.-H., & Hedley, A. J. (2005). Correlation among physical impairments, pain, disability, and patient satisfaction in patients with chronic neck pain. *Archives of Physical Medicine and Rehabilitation, 86*(3), 534–540. http://doi.org/10.1016/j.apmr.2004.02.030

Cole, G. K., Nigg, B. M., Ronsky, J. L., & Yeadon, M. R. (1993). Application of the joint coordinate system to three-dimensional joint attitude and movement representation: a standardization proposal. *Journal of Biomechanical Engineering, 115*(4A), 344–349.

Comerford, M. J., & Mottram, S. L. (2001). Movement and stability dysfunction--contemporary developments. *Manual Therapy, 6*(1), 15–26. http://doi.org/10.1054/math.2000.0388

Cooper, A., Chhina, H., Howren, A., & Alvarez, C. (2014). The contralateral foot in children with unilateral clubfoot, is the unaffected side normal? *Gait & Posture, 40*(3), 375–380. http://doi.org/10.1016/j.gaitpost.2014.05.004

Curtze, C., Hof, A. L., Otten, B., & Postema, K. (2010). Balance recovery after an evoked forward fall in unilateral transtibial amputees. *Gait & Posture, 32*(3), 336–341. http://doi.org/10.1016/j.gaitpost.2010.06.005

Deng, H., Durfee, W. K., Nuckley, D. J., Rheude, B. S., Severson, A. E., Skluzacek, K. M., et al. (2012). Complex versus simple ankle movement training in stroke using telerehabilitation: a randomized controlled trial. *Physical Therapy, 92*(2), 197–209. http://doi.org/10.2522/ptj.20110018

Dietz, V., Zijlstra, W., & Duysens, J. (1994). Human neuronal interlimb coordination during split-belt locomotion. *Experimental Brain Research Experimentelle Hirnforschung Expérimentation Cérébrale, 101*(3), 513–520.

Duysens, J., & Van de Crommert HW. (1998). Neural control of locomotion; The central pattern generator from cats to humans. *Gait & Posture, 7*(2), 131–141.

Engín, A. E., & Chen, S. M. (1986). Statistical data base for the biomechanical properties of the human shoulder complex--I: Kinematics of the shoulder complex. *Journal of Biomechanical Engineering, 108*(3), 215–221.

Favre, J., Jolles, B. M., Aissaoui, R., & Aminian, K. (2008). Ambulatory measurement of 3D knee joint angle, *41*(5), 1029–1035. http://doi.org/10.1016/j.jbiomech.2007.12.003

Favre, J., Luthi, F., Jolles, B. M., Siegrist, O., Najafi, B., & Aminian, K. (2006). A new ambulatory system for comparative evaluation of the three-dimensional knee kinematics, applied to anterior cruciate ligament injuries. *Knee Surgery, Sports Traumatology, Arthroscopy : Official Journal of the ESSKA, 14*(7), 592–604. http://doi.org/10.1007/s00167-005-0023-4

Fayad, F., Roby-Brami, A., Gautheron, V., Lefevre-Colau, M.-M., Hanneton, S., Fermanian, J., et al. (2008). Relationship of glenohumeral elevation and 3-dimensional scapular kinematics with disability in patients with shoulder disorders. *Journal of Rehabilitation Medicine, 40*(6), 456–460. http://doi.org/10.2340/16501977-0199

Grimston, S. K., Nigg, B. M., Hanley, D. A., & Engsberg, J. R. (1993). Differences in ankle joint complex range of motion as a function of age. *Foot and Ankle, 14*(4), 215–222.

Grood, E. S., & Suntay, W. J. (1983). A joint coordinate system for the clinical description of three-dimensional motions: application to the knee. *Journal of Biomechanical Engineering, 105*(2), 136–144.

Hanratty, C. E., McVeigh, J. G., Kerr, D. P., Basford, J. R., Finch, M. B., Pendleton, A., & Sim, J. (2012). The effectiveness of physiotherapy exercises in subacromial impingement syndrome: a systematic review and meta-analysis. *Seminars in Arthritis and Rheumatism, 42*(3), 297–316. http://doi.org/10.1016/j.semarthrit.2012.03.015

Henriksen, M., Alkjaer, T., Simonsen, E. B., & Bliddal, H. (2009). Experimental muscle pain during a forward lunge--the effects on knee joint dynamics and electromyographic activity. British Journal of Sports Medicine, 43(7), 503–507. http://doi.org/10.1136/bjsm.2008.050393

Heyrman, L., Feys, H., Molenaers, G., Jaspers, E., Monari, D., Meyns, P., & Desloovere, K. (2013). *Gait & Posture, 38*(4), 770–776. http://doi.org/10.1016/j.gaitpost.2013.03.019

Hill, A. M., Bull, A. M. J., Wallace, A. L., & Johnson, G. R. (2008). Qualitative and quantitative descriptions of glenohumeral motion. *Gait & Posture, 27*(2), 177–188. http://doi.org/10.1016/j.gaitpost.2007.04.008

Hodges, P. W., & Moseley, G. L. (2003). Pain and motor control of the lumbopelvic region: effect and possible mechanisms. *Journal of Electromyography and Kinesiology : Official Journal of the International Society of Electrophysiological Kinesiology, 13*(4), 361–370.

Hof, A. L. (2007). The equations of motion for a standing human reveal three mechanisms for balance, *40*(2), 451–457.

Horak, F. B., & Nashner, L. M. (1986). Central programming of postural movements: adaptation to altered support-surface configurations. *Journal of Neurophysiology, 55*(6), 1369–1381.

Jenkyn, T. R., Hunt, M. A., Jones, I. C., Giffin, J. R., & Birmingham, T. B. (2008). Toe-out gait in patients with knee osteoarthritis partially transforms external knee adduction moment into flexion moment during early stance phase of gait: a tri-planar kinetic mechanism., *41*(2), 276–283. http://doi.org/10.1016/j.jbiomech.2007.09.015

Kalman, R. E. (1960). A New Approach to Linear Filtering and Prediction Problems, J. *J Basic Eng*.

Kapron, A. L., Aoki, S. K., Peters, C. L., Maas, S. A., Bey, M. J., Zauel, R., & Anderson, A. E. (2014). Accuracy and feasibility of dual fluoroscopy and model-based tracking to quantify in vivo hip kinematics during clinical exams. *Journal of Applied Biomechanics, 30*(3), 461–470. http://doi.org/10.1123/jab.2013-0112

Karduna, A. R., McClure, P. W., Michener, L. A., & Sennett, B. (2001). Dynamic Measurements of Three-Dimensional Scapular Kinematics: A Validation Study. *Journal of Biomechanical Engineering, 123*(2), 184. http://doi.org/10.1115/1.1351892

Kasten, P., Rettig, O., Loew, M., Wolf, S., & Raiss, P. (2009). Three-dimensional motion analysis of compensatory movements in patients with radioulnar synostosis performing activities of daily living. Journal of Orthopaedic Science, 14(3), 307–312. http://doi.org/10.1007/s00776-009-1332-0

Kernozek, T. W., Torry, M. R., & Iwasaki, M. (2008). Gender differences in lower extremity landing mechanics caused by neuromuscular fatigue. *The American Journal of Sports Medicine, 36*(3), 554–565. http://doi.org/10.1177/0363546507308934

Kiernan, D., Malone, A., Brien, T. O., & Simms, C. K. (2014). A 3-dimensional rigid cluster thorax model for kinematicmeasurements during gait, *47*(6), 1499–1505. http://doi.org/10.1016/j.jbiomech.2014.02.020

Kim, Y. K., Kim, Y. H., & Im, S. J. (2011). Inter-joint coordination in producing kicking velocity of taekwondo kicks. *Journal of Sports Science & Medicine, 10*(1), 31–38.

King, J., Harding, E., & Karduna, A. (2013). The Shoulder and Elbow Joints and Right and Left Sides Demonstrate Similar Joint Position Sense. *Journal of Motor Behavior, 45*(6), 479–486. http://doi.org/10.1080/00222895.2013.832136

Lambrecht, J. M., & Kirsch, R. F. (2014). Miniature low-power inertial sensors: promising technology for implantable motion capture systems. *IEEE Transactions on Neural Systems and Rehabilitation Engineering : a Publication of the IEEE Engineering in Medicine and Biology Society, 22*(6), 1138–1147. http://doi.org/10.1109/TNSRE.2014.2324825

Leardini, A., Chiari, L., Croce, Della, U., & Cappozzo, A. (2005). Human movement analysis using stereophotogrammetry. Part 3. Soft tissue artifact assessment and compensation. *Gait & Posture, 21*(2), 212–225. http://doi.org/10.1016/j.gaitpost.2004.05.002

Lempereur, M., Brochard, S., Leboeuf, F., & Rémy-Néris, O. (2014). Validity and reliability of 3D marker based scapular motion analysis: a systematic review. *Journal of Biomechanics, 47*(10), 2219–2230. http://doi.org/10.1016/j.jbiomech.2014.04.028

Lempereur, M., Brochard, S., Mao, L., & Rémy-Néris, O. (2012). Validity and reliability of shoulder kinematics in typically developing children and children with hemiplegic cerebral palsy. *Journal of Biomechanics, 45(*11), 2028–2034. http://doi.org/10.1016/j.jbiomech.2012.05.020

Levasseur, A., Tétreault, P., de Guise, J., Nuño, N., & Hagemeister, N. (2007). The effect of axis alignment on shoulder joint kinematics analysis during arm abduction. *Jclb, 22*(7), 758–766. http://doi.org/10.1016/j.clinbiomech.2007.04.009

Lewinson, R. T., Worobets, J. T., & Stefanyshyn, D. J. (2014). The relationship between maximal hip abductor strength and resultant loading at the knee during walking. Proceedings of the Institution of Mechanical Engineers Part H, *Journal of Engineering in Medicine, 228*(12), 1258–1263. http://doi.org/10.1177/0954411914562490

Lin, C.-F., Hua, S.-H., Huang, M.-T., Lee, H.-H., & Liao, J.-C. (2015). Biomechanical analysis of knee and trunk in badminton players with and without knee pain during backhand diagonal lunges. *Journal of Sports Sciences, 1–11*. http://doi.org/10.1080/02640414.2014.990492

Lopes, A. D., Hespanhol Júnior, L. C., Yeung, S. S., & Costa, L. O. P. (2012). What are the main running-related musculoskeletal injuries? A Systematic Review. *Sports Medicine (Auckland, N.Z.), 42*(10), 891–905. http://doi.org/10.2165/11631170-000000000-00000

Ludewig, P. M., & Cook, T. M. (2000). Alterations in shoulder kinematics and associated muscle activity in people with symptoms of shoulder impingement. Physical Therapy, 80(3), 276–291.

Ludewig, P. M., Phadke, V., Braman, J. P., Hassett, D. R., Cieminski, C. J., & LaPrade, R. F. (2009). Motion of the shoulder complex during multiplanar humeral elevation. The Journal of Bone and Joint Surgery, 91(2), 378–389. http://doi.org/10.2106/JBJS.G.01483

Luinge, H. J., & Veltink, P. H. (2005). Measuring orientation of human body segments using miniature gyroscopes and accelerometers. *Medical and Biological Engineering and Computing, 43*(2), 273–282.

Madgwick, S. O. H., Harrison, A. J. L., & Vaidyanathan, A. (2011). Estimation of IMU and MARG orientation using a gradient descent algorithm. IEEE ... International Conference on Rehabilitation Robotics : [Proceedings], 2011, 5975346. http://doi.org/10.1109/ICORR.2011.5975346

Matsui, K., Shimada, K., & Andrew, P. D. (2006). Deviation of skin marker from bone target during movement of the scapula. Journal of Orthopaedic Science, 11(2), 180–184. http://doi.org/10.1007/s00776-005-1000-y

Mazzà, C., Donati, M., McCamley, J., Picerno, P., & Cappozzo, A. (2012a). An optimized Kalman filter for the estimate of trunk orientation from inertial sensors data during treadmill walking. *Gait & Posture, 35*(1), 138–142. http://doi.org/10.1016/j.gaitpost.2011.08.024

Mazzà, C., Donati, M., McCamley, J., Pietro Picerno, & Cappozzo, A. (2012b). An optimized Kalman filter for the estimate of trunk orientation from inertial sensors data during treadmill walking. *Gait & Posture, 35*(1), 138–142. http://doi.org/10.1016/j.gaitpost.2011.08.024

McLean, S. G., Lucey, S. M., Rohrer, S., & Brandon, C. (2010). Knee joint anatomy predicts high-risk in vivo dynamic landing knee biomechanics. *Clinical Biomechanics (Bristol, Avon), 25*(8), 781–788. http://doi.org/10.1016/j.clinbiomech.2010.06.002

Meyer, K. E., Saether, E. E., Soiney, E. K., Shebeck, M. S., Paddock, K. L., & Ludewig, P. M. (2008). Three-dimensional scapular kinematics during the throwing motion. *Journal of Applied Biomechanics, 24*(1), 24–34.

Nha, K. W., Dorj, A., Feng, J., Shin, J. H., Kim, J. I., Kwon, J. H., et al. (2013). Application of computational lower extremity model to investigate different muscle activities and joint force patterns in knee osteoarthritis patients during walking. *Computational and Mathematical Methods in Medicine, 2013,* 314280. http://doi.org/10.1155/2013/314280

Oberländer, K. D., Brüggemann, G.-P., Höher, J., & Karamanidis, K. (2012). Reduced knee joint moment in ACL deficient patients at a cost of dynamic stability during landing. *Journal of Biomechanics, 45*(8), 1387–1392. http://doi.org/10.1016/j.jbiomech.2012.02.029

Oberländer, K. D., Brüggemann, G.-P., Höher, J., & Karamanidis, K. (2013). Altered landing mechanics in ACL-reconstructed patients. *Medicine & Science in Sports & Exercise, 45*(3), 506–513. http://doi.org/10.1249/MSS.0b013e3182752ae3

Oberländer, K. D., Brüggemann, G.-P., Höher, J., & Karamanidis, K. (2014). Knee mechanics during landing in anterior cruciate ligament patients: A longitudinal study from pre- to 12 months post-reconstruction. *Clinical Biomechanics (Bristol, Avon), 29*(5), 512–517. http://doi.org/10.1016/j.clinbiomech.2014.03.014

Oliveira, A. S., Silva, P. B., Lund, M. E., Gizzi, L., Farina, D., & Kersting, U. G. (2013). Effects of perturbations to balance on neuromechanics of fast changes in direction during locomotion. *PLoS ONE, 8*(3), e59029. http://doi.org/10.1371/journal.pone.0059029

Pandy, M. G., & Andriacchi, T. P. (2010). Muscle and joint function in human locomotion. *Annual Review of Biomedical Engineering, 12(*1), 401–433. http://doi.org/10.1146/annurev-bioeng-070909-105259

Papannagari, R., Gill, T. J., Defrate, L. E., Moses, J. M., Petruska, A. J., & Li, G. (2006). In vivo kinematics of the knee after anterior cruciate ligament reconstruction: a clinical and functional evaluation. *The American Journal of Sports Medicine, 34*(12), 2006–2012. http://doi.org/10.1177/0363546506290403

Peaden, A. W., & Charles, S. K. (2014). Dynamics of wrist and forearm rotations. *Journal of Biomechanics, 1–7.* http://doi.org/10.1016/j.jbiomech.2014.01.053

Pearcy, M. J., & Hindle, R. J. (1989). New method for the non-invasive three-dimensional measurement of human back movement. *Jclb, 4*(2), 73–79. http://doi.org/10.1016/0268-0033(89)90042-9

Peter, W. F., Dekker, J., Tilbury, C., Tordoir, R. L., Verdegaal, S. H. M., Onstenk, R., et al. (2015). The association between comorbidities and pain, physical function and quality of life following hip and knee arthroplasty. *Rheumatology International, 1–9*. http://doi.org/10.1007/s00296-015-3211-7

Petersen, J., Nielsen, R. O., Rasmussen, S., & Sørensen, H. (2014). Comparisons of increases in knee and ankle joint moments following an increase in running speed from 8 to 12 to 16km·h(-1.). *Clinical Biomechanics (Bristol, Avon), 29(*9), 959–964. http://doi.org/10.1016/j.clinbiomech.2014.09.003

Phadke, V., Braman, J. P., LaPrade, R. F., & Ludewig, P. M. (2011). Comparison of glenohumeral motion using different rotation sequences. *Journal of Biomechanics, 44*(4), 700–705. http://doi.org/10.1016/j.jbiomech.2010.10.042

Rao, S., Saltzman, C., & Yack, H. J. (2006). Ankle ROM and stiffness measured at rest and during gait in individuals with and without diabetic sensory neuropathy. *Gait & Posture, 24*(3), 295–301. http://doi.org/10.1016/j.gaitpost.2005.10.004

Resende, R. A., Deluzio, K. J., Kirkwood, R. N., Hassan, E. A., & Fonseca, S. T. (2014). Increased unilateral foot pronation affects lower limbs and pelvic biomechanics during walking. *Gait & Posture.* http://doi.org/10.1016/j.gaitpost.2014.10.025

Robert, T., Rouard, A., & Seifert, L. (2013). Biomechanical analysis of the strike motion in ice-climbing activity. *Computer Methods in Biomechanics and Biomedical Engineering, 16*(sup1), 90–92. http://doi.org/10.1080/10255842.2013.815890

Roetenberg, D. (2006). Inertial and magnetic sensing of human motion.

Roetenberg, D., Slycke, P. J., & Veltink, P. H. (2007). Ambulatory position and orientation tracking fusing magnetic and inertial sensing. *IEEE Transactions on Bio-Medical Engineering, 54*(5), 883–890. http://doi.org/10.1109/TBME.2006.889184

Sabatini, A. M. (2006). Quaternion-Based Extended Kalman Filter for Determining Orientation by Inertial and Magnetic Sensing. IEEE Transactions on Bio-Medical Engineering, 53(7), 1346–1356. http://doi.org/10.1109/TBME.2006.875664

Schnorenberg, A. J., Slavens, B. A., Wang, M., Vogel, L. C., Smith, P. A., & Harris, G. F. (2014). Biomechanical model for evaluation of pediatric upper extremity joint dynamics during wheelchair mobility. *Journal of Biomechanics, 47*(1), 269–276. http://doi.org/10.1016/j.jbiomech.2013.11.014

Schuind, F., An, K. N., Cooney, W. P., & Garcia-Elias, M. (1994). Advances in the biomechanics of the hand and wrist. New York : Plenum Press.

Shaheen, A. F., Villa, C., Lee, Y.-N., Bull, A. M. J., & Alexander, C. M. (2013). Scapular taping alters kinematics in asymptomatic subjects. *Journal of Electromyography and Kinesiology : Official Journal of the International Society of Electrophysiological Kinesiology, 23*(2), 326–333. http://doi.org/10.1016/j.jelekin.2012.11.005

Sherman, S. L., Plackis, A. C., & Nuelle, C. W. (2014). Patellofemoral anatomy and biomechanics. *Clinics in Sports Medicine, 33*(3), 389–401. http://doi.org/10.1016/j.csm.2014.03.008

Shull, P. B., Jirattigalachote, W., Hunt, M. A., Cutkosky, M. R., & Delp, S. L. (2014). Quantified self and human movement: A review on the clinical impact of wearable sensing and feedback for gait analysis and intervention, 1–9. http://doi.org/10.1016/j.gaitpost.2014.03.189

Šenk, M., & Cheze, L. (2006). Rotation sequence as an important factor in shoulder kinematics. *Jclb, 21 Suppl 1*, S3–8. http://doi.org/10.1016/j.clinbiomech.2005.09.007

Tashman, S., Collon, D., Anderson, K., Kolowich, P., & Anderst, W. (2004). Abnormal rotational knee motion during running after anterior cruciate ligament reconstruction. *The American Journal of Sports Medicine, 32*(4), 975–983.

Titterton, D., & Weston, J. L. (2004). *Strapdown Inertial Navigation Technology,* 2nd Edition. IET.

van Arkel, R. J., Modenese, L., Phillips, A. T. M., & Jeffers, J. R. T. (2013). Hip abduction can prevent posterior edge loading of hip replacements. *Journal of Orthopaedic Research : Official Publication of the Orthopaedic Research Society, 31*(8), 1172–1179. http://doi.org/10.1002/jor.22364

van den Bogert, A. J., Smith, G. D., & Nigg, B. M. (1994). In vivo determination of the anatomical axes of the ankle joint complex: an optimization approach. *Journal of Biomechanics, 27*(12), 1477–1488.

Willwacher, S., König, M., Potthast, W., & Brüggemann, G.-P. (2013). Does specific footwear facilitate energy storage and return at the metatarsophalangeal joint in running? *Journal of Applied Biomechanics, 29*(5), 583–592.

Willwacher, S., Regniet, L., Mira Fischer, K., Oberländer, K. D., & Brüggemann, G.-P. (2014). The effect of shoes, surface conditions and sex on leg geometry at touchdown in habitually shod runners. *Footwear Science,* 1–10. http://doi.org/10.1080/19424280.2014.896952

Wu, G. (2002). ISB recommendation on definitions of joint coordinate system of various joints for the reporting of human joint motion—part I: ankle, hip, and spine, 6.

Wu, G., & Cavanagh, P. R. (1995). ISB recommendations for standardization in the reporting of kinematic data, 28(10), 1257–1261.

Wu, G., der Helm, van, F. C. T., Veeger, H. E. J. D., Makhsous, M., Van Roy, P., Anglin, C., et al. (2005). ISB recommendation on definitions of joint coordinate systems of various joints for the reporting of human joint motion--Part II: shoulder, elbow, wrist and hand. *Journal of Biomechanics, 38*(5), 981–992.

Xu, X., Qin, J., Catena, R. D., Faber, G. S., & Lin, J.-H. (2013). Effect of aging on inter-joint synergies during machine-paced assembly tasks. *Experimental Brain Research Experimentelle Hirnforschung Expérimentation Cérébrale, 231*(2), 249–256. http://doi.org/10.1007/s00221-013-3688-9

Zhou, H., Stone, T., Hu, H., & Harris, N. (2008). Use of multiple wearable inertial sensors in upper limb motion tracking. *Medical Engineering & Physics, 30*(1), 123–133. http://doi.org/10.1016/j.medengphy.2006.11.010

About The Author

Kai Daniel Oberländer, Dr. rer. nat.

Born in Germany, Dr. Oberländer studied Sport-science and Mathematics at the University of Koblenz-Landau (Germany). In 2008 he moved to Cologne and started his doctoral thesis at the Institute of Biomechanics and Orthopeadics at the German Sport University in Cologne led by Prof. Dr. Gert-Peter Brüggemann, further he received a two year scholarship (DFG). In 2010 he became scientific assistant at Institute of Biomechanics and Orthopeadics. Currently Dr. Oberländer is a sought after consultant for biomedical product development with more than seven years of experience. Besides his work for European and U.S. clients, he holds a deputy professorship for sports biomedical engineering and is one of the founders of Protendon GmbH & Co. KG. This company specializes in building applications for neuromuscular assessments. Dr. Oberländer's deep knowledge in wearable sensor technology and biomechanical analysis workflows makes him a unique asset to drive product innovation and market placement.